Lawrence Berkeley National Laboratory

Title
THE TEXTURE OF DIRECTIONALLY SOLIDIFIED Al-CuAl2 EUTECTIC ALLOY

Permalink
https://escholarship.org/uc/item/3qd212h7

Author
Valero, Leopoldo.

Publication Date
1978

THE TEXTURE OF DIRECTIONALLY SOLIDIFIED Al-CuAl$_2$ EUTECTIC ALLOY

Leopoldo Valero
(M. S. thesis)

January 1978

DISCLAIMER

THE TEXTURE OF DIRECTIONALLY SOLIDIFIED Al-CuAl$_2$ EUTECTIC ALLOY

Leopoldo Valero

ABSTRACT

An experiment was conducted to determine the texture of an Ai-CuAl$_2$ eutectic alloy unidirectionally solidified at 12.9 µm/s under a temperature gradient of 70.7°C/cm. Directional solidification produced a parallel well aligned microstructure with an interlamellar spacing of 2.73 µm. The lamellae exhibited a strong preferred orientation or texture. An x-ray diffractometer method was used to obtain the data and pole figures corresponding to each of the two solid phases were plotted. The pole intensities were represented in terms of "times random" units. The results of this investigation are summarized as follows:

Interfacial relationships $\qquad\qquad$ (111) K || (21$\bar{1}$) θ

$\qquad\qquad\qquad\qquad\qquad\qquad\qquad$ [1$\bar{1}$0] K || [1$\bar{2}$0] θ

Growth direction close to $\quad$ [$\bar{1}\bar{1}$2] K

Dedicated to my daughters Graciela and Marcia to whom I owe
so many hours of play.

ACKNOWLEDGEMENTS

TABLE OF CONTENTS

I. INTRODUCTION

The directional solidification of eutectic alloys offers an attractive means of producing in a single operation a composite material directly from the melt and thus avoiding many of the complex processing operations related to the production of synthetic composites (1).

The two phases in a simple binary eutectic normally grow perpendicular to the liquid/solid interface. If a eutectic is unidirectionally frozen, a composite microstructure is produced with an aligned reinforcing phase in a ductile matrix. The resulting microstructure has an excellent isothermal stability, since the phases are in thermodynamic equilibrium with each other up to the melting point of the alloy (2).

Eutectic alloys solidified in this manner show the special mechanical properties which are associated with reinforced composite materials and also exhibit desirable physical properties. Examples are the Al-Al$_3$Ni eutectic which has an Al matrix reinforced with intermetallic Al$_3$Ni fibres that deform elastically to failure (3), and the InSb-NiSb eutectic alloy used commercially on account of its electrical properties. This material has the highest magnetoresistance known and it is used as a magnetic field sensor, as a current transducer or as a contactless switch (4).

The properties of the eutectic alloys are highly anisotropic, therefore a knowledge of the crystallographic relationships developed between the two phases during solidification is essential. Ideally certain directions in one or both phases should lie parallel to the growth direction and a definite interphase relationship should exist.

As grown these directionally solidified eutectics are not perfect duplex single crystals and are best described in terms of a strong preferred orientation or texture.

The two phases in a unidirectionally frozen eutectic, solidify either as rods of one phase within a continuous matrix of the other or as alternate lamellae of each phase. The separation of the phases λ, varies with growth rate R and decreases with increasing growth rate according to the relationship $\lambda^2 R$ = Constant (21). The eutectic will freeze in that form which has the minimal interface surface energy for any given separation. Rods are favored when the volume fraction of the minor phase is less than 0.28, while a lamellar arrangement would be more probable for a higher volume fraction of the minor phase (14).

The lamellar eutectic between the aluminum solid solution K phase (Al-5.7% Cu) and the intermetallic compound $CuAl_2$ (θ phase) has been studied extensively (references 8-12 and 23-32). The texture and inter-phase relationships reported have been the object of controversy among different investigators (12, 25-28). In this work it is intended to find the crystallographic relationships existing between the two phases present and to verify to what extent these results agree with those already present in the literature.

II. EUTECTIC GRAINS

The term "grain" to describe distinguishable regions in a eutectic microstructure, analogous to the single crystalline grains in a single phase alloy was established by Rosenhain and Tucker who studied the lamellar structure of the Pb-Sn eutectic in 1909 (5,6). In 1937 Straumanis and Brakss (7) were the first to use a directional solidification technique to obtain parallel lamellae in a form suitable for x-ray examination. They examined the orientation relationships between the two phases and concluded that in a binary lamellar eutectic each phase maintains a constant orientation throughout a eutectic grain and that a eutectic grain could be regarded as two interpenetrating single crystals, one for each phase.

Recently the concept of a eutectic grain, as described by Straumanis and Brakss has had to be modified to account for the presence of subgrains (8,9) and for progressive changes which have been observed in the crystallographic and metallographic angular relationships within a region where continuous growth has taken place from a single nucleation point (10, 11, 12). It has been found useful then, to consider a eutectic single crystal as a region of substantially uniform crystal orientation separated from other grains by identifiable boundaries (Figures 1 and 5).

A. EUTECTIC SOLIDIFICATION

In a binary phase diagram the eutectic composition is found at the intersection of two liquidus lines that slope in opposite directions.

At this point (defined by both the eutectic temperature and the eutectic composition) a single liquid phase is in dynamic equilibrium with two distinct solid phases (13). The transformation from a liquid to two solids is called a eutectic transformation. A necessary condition for eutectic solidification to occur is that the solubilities of the two phases be limited. Each species of atoms should have a strong preference for its own crystal structure and when an intermediate phase is involved it must also have limited solubility for the other phase (15).

A great variety of structures have been observed in the metallographic examination of binary eutectics. All of these structures, no matter how complex they may be, exhibit a common characteristic: two phases produced during eutectic solidification can always be seen under the microscope (8, 15).

B. Eutectic Microstructures

A classification of eutectic microstructures based on their mode of crystallization is due to Scheil (16) who in 1959 published a final review of his extensive work in eutectic microstructures which he had started in 1934. This classification was developed from metallographic studies of the freezing behavior and in part from the development of a model for the steady state growth of a lamellar eutectic (next section). All binary eutectics microstructures were divided into two classes: normal and abnormal. When a normal structure was formed it was usually found that the two solid phases were present in approximately the same proportion by volume, which implied that the liquidus lines were roughly symmetrical about the eutectic point. An abnormal microstructure was

observed almost invariably in those eutectic systems in which the liquidus lines were markedly asymmetric about the eutectic point (5).

Normal microstructures are the lamellar or fibrous types which are formed by the simultaneous growth of the two solid phases. For a normal microstructure to develop the solid phases have to grow at a common interface that forms an extended surface in contact with the melt (22). This pattern is readily observed when a slowly freezing melt is quenched, as described by Weart and Mack (8). The eutectic will solidify with this type of microstructure only if the two solid phases grow at the same linear velocity. Another feature of a normal microstructure, according to Scheil's classification, is that a consistent crystallographic orientation relationship exists between the phases in a given eutectic.

An abnormal microstructure is formed when the two solid phases are prevented from growing at equal linear velocity. A mixture of phases may be formed and there is a corresponding wide variety of details observed in abnormal microstructures. The faster growing phase is usually the one present in smaller proportion by volume. This phase grows freely into the melt in a branching which resembles a dendritic pattern. The lagging phase crystallizes from the melt trapped between the branches (6).

Tiller (18) and Jackson and Hunt (21) investigated the possibilities of expressing in mathematical terms the conditions necessary for the formation of the eutectic solidification microstructures described by Scheil. The theories developed have worked fairly well when applied to lamellar growth of eutectics.

C. Growth of a Lamellar Eutectic

It has been shown experimentally (7, 15, 19) that the two phases in a lamellar eutectic grow simultaneously and that each lamella has its own solid-liquid interface. Scheil (33) showed that undercooling below the eutectic temperature is essential for the growth of a lamellar eutectic. If the liquidus lines in a binary phase diagram with components A and B are extended below the eutectic temperature, a region will be enclosed in which the liquid is supersaturated with respect to the two phases α and β. In this region simultaneous growth of the two solid phases from the melt is thermodynamically possible. During the growth of an α lamella atoms of B are continually rejected into the melt at the solid-liquid interface, therefore the liquid in contact with the α interface is enriched in the major component of the adjacent lamella. Conversely the melt in contact with the β lamella is poor in component B. Transverse diffusion between the two components is taking place with the corresponding changes in composition. No such composition variation is possible at the equilibrium temperature and some undercooling is necessary for lamellar growth to occur.

Zener in his analysis of the growth of pearlite (34) laid the foundations for the theoretical work in the growth of lamellar eutectics. He stated that the solid - solid interfacial energy between the α and β lamellae must be supplied from the energy released in freezing and that the minimum possible undercooling is such that the free energy difference per unit mass between solid and liquid is equal to the interfacial energy. Zener postulated that at a given undercooling the growth rate was the

maximum possible and predicted that the product of the growth velocity v and the square of the lamellar spacing λ should be constant. Brandt (35) obtained an approximate solution to the diffusion equation assuming that the interface between the lamellae and austenite was sinusoidal. Hillert (36) extended the work of Zener and found a solution to the diffusion equation assuming the interface to be plane. Taking surface energy into account, and using Zener's maximum condition, he calculated an approximate shape of the interface.

Tiller (18) applied some of the ideas of the growth of pearlite to the growth of eutectics. He proposed a minimum undercooling condition to replace the maximum growth rate condition by Zener. Jackson and Hunt (21) derived the steady-state solution to the diffusion equation for a lamellar eutectic growing with a plane interface. Expressions were obtained for the average composition at the interface and the average curvature of the interface similar in form to those equations derived by Zener (34) and Tiller (18). Jackson and Hunt adopted Hillert's planar solid-liquid interface approximation and used Brandt's solution to the diffusion equation in the form:

$$C = Ce + C_\infty + B_o \exp\left(\frac{-RZ}{D}\right) + \sum_{n=1}^{\infty} B_n \cos\left(\frac{n\pi x}{S_\alpha + S_\beta}\right) \exp\left(\frac{-n\pi Z}{S_\alpha + S_\beta}\right) \qquad \text{(Eq. 1)}$$

where C is the melt composition at any point X, Z (the solid-liquid interface is represented as advancing in the Z direction as freezing progresses, the X direction is parallel to the interface, transverse to the lamellae). The term (Ce + C∞) is regarded as the initial melt

composition, allowing for a deviation C_α from the equilibrium eutectic

composition, C_e. S_α and S_β are the half-widths of the α and β lamellae,

therefore $2(S_\alpha + S_\beta) = \lambda$. R is the growth rate or the rate of advance

of the solid liquid interface and D is the diffusion coefficient in the

melt. The last term accounts for the variation of composition in the X

direction at a distance Z from the interface. B_o and B_n are Fourier

coefficients.

Average values for interface curvature, for composition, and under-

cooling of the liquid in front of each face were obtained using

Equation 1. It was found that at the extremum condition of either

maximum growth velocity or growth at minimum undercooling, the following

relationships apply:

$$\lambda^2 R = const \qquad (eq. 2)$$
$$\frac{\Delta T^2}{R} = const \qquad (eq. 3)$$
$$\Delta T \lambda = const \qquad (eq. 4)$$

Jackson and Hunt's analysis is an accurate description of normal

eutectic growth and is considered the turning point from qualitative

to quantitative research in eutectic solidification.

The various mathematical analyses on lamellar growth of eutectics

predict that this type of microstructure will be favored to grow if

the two solid phases are oriented crystallographically in such a way

as to minimize the interfacial energy between the lamellae.

III. THE Al-CuAl$_2$ EUTECTIC ALLOY

A. Solidification and Microstructure

The Al-Cu pseudo binary phase diagram showing the aluminum rich side is presented in Figure 2. The eutectic temperature is equal to 548°C and the eutectic composition is 33.3 wt % Cu and 66.7 wt % Al. The eutectic is formed between the K phase which is a substitutional solid solution of Cu in Al (Al-5.7 % Cu) with a face centered cubic unit cell, where A_o = 4.04 A$^\circ$ and the θ phase an intermetallic compound (CuAl$_2$) with a body centered tetragonal unit cell, where A_o = 6.04 A$^\circ$ and C_o = 4.86 A$^\circ$ (Figures 3a and 3c).

The solidification experiments conducted by Kraft and Albright (23) showed that the Al-CuAl$_2$ eutectic alloy, when unidirectionally frozen can be forced to solidify as parallel lamellae throughout a relative large volume, if the solidification parameters are controlled appropriately. These variables are the temperature gradient at the solid-liquid interface (G), the growth rate (R) and the concentration of impurities. When the ratio G/R is less than a critical value or if excess impurity is present, a eutectic colony microstructure is formed. The impurities, being rejected by both phases of the eutectic, cause the liquid in front of the advancing solid-liquid interface to become constitutionally supercooled below the equilibrium liquidus temperature. A constitutionally supercooled layer in turn stabilizes a cellular rather than a planar interface and a cellular solid-liquid interface leads to the formation of eutectic colonies (8, 18). In a cellular or eutectic colony structure the two phases of the eutectic remain lamellar within

a cell, but they do not grow parallel to each other and diverge towards
the colony boundaries in a fan-like arrangement (24). If the G/R ratio
is greater than the critical value, a continuous lamellar structure is
formed in which the two phases lie approximately parallel to each other
within each individual grain (Figures 4 and 5). This microstructure
exhibits imperfections termed lamellar faults, a defect that appears to
be common to all lamellar eutectics. Lamellar faults are caused by the
nucleation of an extra lamella and are very similar to edge dislocation
models in crystals.

Kraft and Albright also noticed that at very slow rate of solidifi-
cation a transverse defect called banding appeared. A single band
usually formed continuously across all grains in one ingot. The bands
were observed to be convex towards the liquid which indicated that
banding was a phenomenon associated with the liquid-solid interface. No
satisfactory explanation of the origin of the structure was given.
Chadwick (24) demonstrated that the banding structure can be due to minor
perturbations on otherwise steady state conditions of solidification.

Chadwick (24) investigated the variation of the micro-morphology of
the eutectic with growth conditions. Eutectics were made from slightly
impure and from zone-refined metals. In alloys which were prepared from
Cu and Al of 99.999 % purity, a colony structure developed when R was
faster than 15 cm/hour. No cellular structure was observed in an
eutectic alloy made from zone-refined Cu and Al, which confirmed the fact
that the presence of small quantities of impurity elements is a necessary
condition for a colony eutectic microstructure to form. Chadwick also
studied the effect of growth rate on the inter-lamellar spacing using an

imposed constant temperature gradient of 70° C/cm. A parallel lamellar structure was obtained at values of R between 10 and 1 cm/hour, the only irregularities being lamellar faults. Measurements of λ, in this range, confirmed the existence of the relationship $\lambda = AR^{-1/2}$, where A is a constant. This result validated then the theoretical predictions made by Tiller (18) and by Jackson and Hunt (equation 2).

B. Crystallography

The lamellar structure of the Al-CuAl$_2$ eutectic alloy follows the general pattern of this mode of solidification which is characterized by a preferred crystal orientation between the two solid phases stabilized by a selection of a low energy interface during growth (33).

A planar interface between two crystals has five degrees of freedom, three arising from the relative orientation of the two grains and two from the orientation of the boundary surface itself with respect to the two grains (38). These five degrees of freedom can be specified by two statements (25):

Lamellar habit plane $\quad || (hkl)_\alpha || (hkl)_\beta \qquad$ (A)

$$[uvw]_\alpha || [uvw]_\beta \qquad \text{(B)}$$

(A) specifies the crystallographic planes that are in contact at the interface and (B) fixes the relative rotation of the two crystals about an axis normal to the interface, since the directions in statement (B) are chosen to lie within the planes of statement (A). These two statements do not include the growth direction, which is assumed to lie within the lamellar interfaces.

Usually all five degrees of freedom in eutectics crystals have not been established, and the results are presented in the form:

$$(hkl)_{\alpha} \parallel (hkl)_{\beta} \qquad (C)$$

$$[uvw]_{\alpha} \parallel [uvw]_{\beta} \qquad (D)$$

here the directions indicated in (D) lie within the respective planes of statement (C) and nothing is stated about the habit plane which could cut the unit cells at any arbitrary angle, because two degrees of freedom are not specified.

Table 1 shows the results of a literature survey on the crystallography of the $Al-CuAl_2$ eutectic where the crystallographic relationships between the two phases are presented in the forms described above. Statements of the type A and B refer to the unidirectionally solidified eutectic (11, 12, 25, 27) and statements of the type C and D can be applied to the pure binary eutectic alloy or to the unidrectionally frozen (26, 27, 29). Kraft (27) reported the following crystallographic relationships for the eutectic:

$$\text{Lamellae} \qquad (111)Al \parallel (211)\ CuAl_2 \qquad (A)$$

$$[10\bar{1}]Al \parallel [1\bar{2}0]\ CuAl_2 \qquad (B)$$

$$(001)Al \parallel (001)\ CuAl_2 \qquad (C)$$

$$[3\bar{1}0]Al \parallel [100]\ CuAl_2 \qquad (D)$$

This is an example of alternative ways of specifying the relative orientation between the unit ceels, depending on the number of degrees of freedom known about the system being investigated.

It can be noticed, by referring to Table 1, that the results reported show disagreement among the investigators and that the experi-

mental conditions, technique used, and speciment preparation were quite different in each case reported. In the case of the interfacial relationships for the unidirectionally solidified $Al-CuAl_2$ eutectic it has been definitely established that the statements:

$$\{111\} \text{ K} \parallel \{211\} \text{ } \theta$$

$$<110> \text{ K} \parallel <210> \text{ } \theta$$

are valid (11, 12, 25). Discrepancies still exist in the growth direction and in the relative position of the habit plane with respect to the two planes of contact. Kraft (25) found that the habit plane was parallel to $\{111\}Al$ and $\{211\}\theta$, Davies and Hellawell (11) found that it was approximately 12° away from these two planes and Cantor and Chadwick (12) reported that the lamellar plane varied in orientation over an angle of about $\pm 8^{\circ}$ and was close to $\{111\}Al$ and $\{211\}\theta$. Cantor and Chadwick stated that the discrepancy in previous results was due to real variations of orientation in the lamellar plane and suggested that the interphase boundary energy is not the sole influence determining growth crystallography. They attributed the variations to local growth fluctuations or anisotropic growth kinetics and found that there is no tendency for progressive change in crystallographic orientation during growth, thus contradicting previous observations that the lamellae spiral continuously during growth (10, 39).

C. Interfacial Structure

It has been shown that the $Al-CuAl_2$ lamellae with the preferred crystallographic relationships discussed previously, are very stable when heated in the solid state (40). This and other similar experiments

(33) have led to the conclusion that the interfaces between lamellae grown unidirectionally under steady-state conditions are configurations of low energy.

The $\{111\}$ Al $||$ $\{211\}\theta$ interface is apparently a low energy configuration for the Al-CuAl$_2$ eutectic. Kraft (25) has demonstrated that this orientation relation produces a very good atomic density matching by observing that in the θ phase the stacking sequence parallel to $\{211\}$ is very unusual. Here four layers of aluminum atoms are grouped together forming almost one single plane (see Figure 3b). All the atoms in this single plane or "puckered" plane would be close enough to exert a bonding force on the atoms in a neighboring $\{111\}$ plane of aluminum, which creates then a stable low energy interface.

Recently, Garmong and Rhodes (30) studied the interfacial structure of the Al-CuAl$_2$ unidirectionally solidified eutectic using electron microscope techniques. Displacement vector analysis, thickness fringe displacement and direct observation gave enough evidence to conclude that the interface is composed of arrays of ledges which provide a low energy configuration to account for structural irregularities found in the system and also provide a mechanism for interfacial migration.

A low energy interface is often interrupted by growth accidents or perturbations such as faults, terminations and bends. These accidents affect the microstructure in two ways: the misorientation of the boundary with respect to the crystals and the misorientation of the crystallography of the two phases with respect to the boundary. According to Garmong and Rhodes, various kinds of defects can be explained in terms of the role played by the ledges. Pure interfacial boundary dis-

locations relieve misfit in the plane of the interface, pure ledges and other types of ledges allow boundary misorientation and crystallographic misorientation. It was concluded that in this system the lamellar interfaces contain appropriate arrays of ledges to produce the observed structural defects while retaining to a great extent the crystallographic relationships between the solid phases which are associated with a low energy interface (30).

IV. EXPERIMENTAL

A. Material Preparation and Characterization

The alloy of eutectic composition was prepared from 99.999 % purity Al and Cu. A ceramic boat of inside dimensions: L = 24 cm, W = 2.0 cm, and H = 1.4 cm was used to grow the eutectic. The sample was place in the boat in a quartz horizontal tube furnace under an argon atmosphere, melted and homogenized at a temperature of about $870^\circ C$. The unidirectional solidification apparatus used in this experiment is described in reference 14. The freezing rate, which is assumed to be equal to the rate of furnace travel, was 12.9 $\mu m/s$, and the measured temperature gradient at the liquid/solid interface was 70.7° C/cm. The weight of the sample was 133.5 gm.

To locate the eutectic grain representative of steady state growth conditions the top and the lateral sides of the solidified ingot were examined under the optical microscope. The eutectic single crystal (Figure 5) was found at about the center portion of the ingot, cut and machine shaped as a rectangular parallelepiped with its sides parallel to the growth direction. The final dimensions of the specimen selected were: L = 1.25 cm, W = 0.60 cm, and H = 0.70 cm.

The specimen was mounted in a plastic material (Koldmount) and then polished and etched for optical microscopy examination. The polishing was done using a 1/o, 2/o, 3/o and 4/o polishing paper lubricated with kerosene, followed by a 1 micron Al-silica cloth on a polishing wheel. The polished surface was then etched with Keller's reagent (10 ml HF, 25 ml HNO_3, 15 ml HCl and 50 ml H_2O) at room temperature with two

successive attacks during 3 second separated by washes under flow of water. Optical microscopy examination revealed the microstructures shown in Fig. 4 which are micrographs taken from the top, transverse and longitudinal sides of the specimen. From these micrographs the sketch of Fig. 5 was constructed which represents a unidirectionally solidified $Al-CuAl_2$ eutectic grain as it would look magnified about 800 times.

B. Instrument and X-ray Texture Determination

The instrument that was available to do this work is shown in Fig. 6a. This instrument provides rotation about the diffractometer axis only (α angle) and two different rotations of the specimen are required for texture determination. It was necessary then to modify the original instrument in order to obtain the second type of rotation needed (β angle). Figure 6b shows the instrument as it was used in reflection, and Fig. 6c is the setup that was utilized in transmission.

The specimen was place in the instrument with the transverse side facing the x-ray source and data was obtained in reflection first, following the procedure outlined in Appendix A. The diffractometer table was allowed to scan from $2\theta = 36.50°$ to $2\theta = 40.00°$ at a speed of $1°/min$. At the same time the recording chart was moving at a speed of 1 in/min while recording the peak intensity profiles arising from the {111} K planes for which $2\theta = 38.40°$ and from the {121} θ planes for which $2\theta = 37.95°$ when $\alpha = 0°$ (Figs. 8 and 9). The x-ray source was CuK_α, operated at a voltage of 40 Kv with a current of 20 ma. A Ni filter was used. To cover the blind region of the pole (Fig. 37) CrK_α radiation was used with a V filter. This tube change made possible to obtain data

for values of α up to $\pm 24^{\circ}$.

After the data in reflection was completed, the specimen was removed from the instrument and mounted in Koldmount to protect it against damage while cutting a sample to be used in transmission. A thin section about 0.0508 cm was cut parallel to the transverse side. This section was mechanically thined down to a final thickness of 0.0089 cm. While doing this operation special care was taken to preserve the surface from which the reflection data had been taken and the removing of material was done on the opposite surface. The transmission data was recorded as explained in Appendix A.

In both cases, readings were taken at increments of 6° for α and 10° for β. α was varied while β kept fixed. The range of α was $-90^{\circ} \leq \alpha < 90^{\circ}$, and the range of β was $-90^{\circ} \leq \beta \leq 90^{\circ}$. α was defined to be positive according to the method of Bragg and Packard (37) (counterclockwise) and β was positive when the specimen was rotated in a clockwise direction.

C. Measurement of the Absorption Factor, μx

A similar procedure to that outlined by Geisler (43) was used to measure the absorption factor, μx. A Lif single crystal was place in the goniometer and oriented to reflect the CuK_{α} radiation. Several counts of the intensity were made and the average was used as the incident intensity I_o, in the absorption equation:

$$\frac{I_x}{I_o} = e^{-\mu x} \qquad \text{(Eq. 5)}$$

the Al-CuAl$_2$ specimen was then placed over the opening in the Geiger

Counter housing and held in place with scotch tape along the edges. The

reduced intensity transmitted by the specimen I$_x$, was measured by averag-

ing counts and from the two measurements μx was calculated.

D. Data Analysis

Figure 9 shows a typical set of data as it was obtained from the

diffractometer recording chart. The most intense peak at a 2θ angle of

38.40° corresponds to the {111} K reflection. As α varies from +12° to

-12° the {121} θ reflection appears to the left of the {111} K, where

2θ=37.95° and when α = -12° the two peaks have merged into one. The

integrated intensities used to plot the pole figures were calculated by

multiplying the measured peak height by the half width of the curve. To

distinguish between the two reflections involved it was necessary to draw

the approximate shape of the peaks as illustrated in Fig. 10.

Data Corrections

a) The calculated intensities were corrected first from the error arising

when two curves are very close together and interact, given a resultant

corresponding to the addition of the two components. Figures 11a and 11b

show the different cases found depending on the ratio of the two peaks.

From these figures a correction factor was derived and Table 3A was con-

structed.

b) Table 3B gives values for correction due to changes in the diffracted

area when β varies. This situation arose because the x-ray beam was

larger than the sample, which in turn was of rectangular shape. Figure 12

is a geometrical representation of the problem, and it was used to derive a correction factor with respect to $\beta = 0°$.

c) The absorption correction factors were calculated using the following equations (37):

i) Reflection Case

$$R_R(\alpha) = \frac{\left\langle 1 + \dfrac{\sin(\theta + \alpha)}{\sin(\theta - \alpha)} \right\rangle \left\langle 1 - \exp\left[-\dfrac{2x}{\sin\theta}\right] \right\rangle}{2\left(1 - \exp\left[-\mu x \left\langle \dfrac{1}{\sin(\theta + \alpha)} + \dfrac{1}{\sin(\theta - \alpha)} \right\rangle \right]\right)}$$ (Eq. 6)

ii) Transmission Case

$$R_T(\alpha) = \frac{\mu x \left\langle 1 - \dfrac{\cos(\theta + \alpha')}{\cos(\theta - \alpha')} \right\rangle \exp\left[-\dfrac{\mu x}{\cos\theta}\right]}{\cos\theta \left\langle \exp\left[-\dfrac{\mu x}{\cos(\theta - \alpha')}\right] - \exp\left[-\dfrac{\mu x}{\cos(\theta + \alpha')}\right] \right\rangle}$$ (Eq. 7)

where $\alpha' = \alpha - 90°$. By making the appropriate substitutions in these two equations the correction factors of Table 3C were found.

d) Transmission data converted to reflection. The formula for the reflected intensity is given by:

$$I_R = \frac{IA}{2\mu}\left[1 - e^{-\frac{2\mu x}{\sin\theta}}\right]$$ (Eq. 8)

and for the transmitted intensity becomes;

$$I_T = I\left[\frac{Ax}{\cos\theta}\, e^{-\frac{\mu x}{\cos\theta}}\right]$$ (Eq. 9)

μx was calculated experimentally to be 1.049. Substituting this value in equations 8 and 9 and combining the following relationship was derived:

$$I_R = 1.36\ I_T$$

To convert data from transmission to reflection it was necessary then to multiply by the factor 1.36.

e) Cr radiation values converted to Cu values. As it was mentioned previously the blind region of the pole figure was covered by changing from CuK_α radiation to CrK_α radiation. This region includes values of $\alpha = 18^o$, 24°, -18°, -24°. To convert Cr values to Cu values the absorption factors were calculated first by using Equation 8 and the corresponding corrections were made. After that a proportionality factor was found by calculating the ratio

$$\frac{CuK_\alpha}{CrK_\alpha}\quad \text{for each } \beta \text{ at } \alpha = 0^o$$

f) Conversion to "Times Random" units. Appendix B describes the procedure followed to calculate the value of $_{hkl}$, the factor by which all the corrected intensities must be divided to express them in "times random" units. This factor was equal to 2258.48 for the {111} K data and 712.83 for the {121} θ data.

For each β a plot of "times random" units vs. α was made. Figures 13a and 13b are examples of these graphs. From these plots a "times random" units table was constructed (Table 4). In this table for each fixed β the values of the corresponding α are tabulated at different

intensity levels. The information from the "times random" units tables was used to draw the pole figures for the {111} K (Figure 15) and for the {121} θ (Figure 16). These pole figures were plotted on a Wulff net following the procedure described by Cullity (41).

V. RESULTS

A unidirectionally frozen Al-CuAl$_2$ eutectic alloy will solidify as parallel lamellae if the solidification parameters are controlled appropriately. A eutectic grain solidified in this manner exhibits a strong preferred orientation or texture. Figure 20 is a transmission x-ray pinhole photograph of the specimen showing the characteristic discontinuities in the Debye rings indicating that preferred orientation is present.

To find the crystallographic relationships for the eutectic, the x-ray diffraction data of Table 2 was recorded. The table indicates which planes were strongly reflected and in analyzing this data it was found that the reflections obtained from both phases were not suitable to obtain a reliable pole figure. To construct a pole figure, in order to find crystallographic relationships between the two phases involved, the reflections selected must be as far apart as possible (40). The (111)K reflection was strong enough but it appears too close to the (121)θ reflection. The (200)K was also observable but it was too weak and its 2θ angle is very close to the value corresponding to the (112)θ (44.72° and 42.59° respectively).

Considering the limitations imposed by the data obtained with the equipment available, it was decided then to assume that the interfacial

relationship $\{111\}$K $||$ $\{121\}$θ was valid and the task was directed to
following the variation of these two reflections throughout the specimen
which was oriented with the growth direction parallel to the x-ray source.
Figure 9 shows a typical set of data obtained and Figure 10 shows that
the two reflections can be resolved without great difficulty knowing that
the 2θ angles are 38.40° for the $\{111\}$K and 37.95° for the $\{121\}$θ.

The pole figures for the two chosen reflections were plotted
(Figs. 15 and 16). For each pole figure five poles were obtained. To
identify the θ phase poles, Table 5 was constructed, which gives the
calculated angles between planes of the form $\{121\}$. The angles between
the maximum points were measured in the pole figure (Table 6) and the
poles were identified and indexed. The proper indexing of the $\{111\}$K
poles was done with the aid of the (112) cubic standard stereographic
projection (Figure 14) which corresponds closely to the $\{111\}$K pole
figure. The signs of the $\{111\}$ K poles were determined by the signs
assigned to the $\{121\}$ θ poles and they had to be consistent with the
measured angles between the maximum points in the pole figure. After the
indexing was completed it was concluded that the growth direction normal
to the eutectic grain was very close to $(\bar{1}\bar{1}2)$ K.

Figure 5 is a sketch of the eutectic grain in which the angles that
the lamellae make with two orthogonal surfaces are indicated (the trans-
verse and the longitudinal sides of the specimen). These measured angles
were used to do a trace analysis (Fig. 19) following the procedure
described by Barrett and Massalski (42). Figure 19 (a) was plotted on
a $(\bar{1}\bar{1}2)$ cubic projection and Figure 19 (b) on a $(\bar{0}\bar{2}2)$ cubic projection,

this last drawing clearly indicating that the lamellae grew parallel to the $[\bar{1}22]$ K and that the plane causing the traces is the $(\bar{1}11)$ K which incidentally is the plane most strongly reflected in the {111} K pole figure. (Figure 15).

The two pole figures were superimposed (figure 17) and the results shown in Figure 18 obtained. The relationships found can be stated as follows:

$$(111) \ K \ || \ (21\bar{1}) \ \theta$$

$$[110] \ K \ || \ [1\bar{2}0] \ \theta$$

Lamellar habit plane approximately 3° from (111) K and $(21\bar{1})$ θ. Grain growth direction close to $[\bar{1}\bar{1}2]$ K. Lamellae growth direction parallel to $[\bar{1}\bar{2}2]$ K.

The data utilized to arrive at these results were expressed in "times random" units. To compute the data an integral is replaced by a double summation (37). This procedure allows the calculation of a quantity designated as J_{hkl}, a factor used to convert the corrected intensities to "times random" units (see Appendix B). When $\Delta\alpha = 6^{\circ}$ and $\Delta\beta = 10^{\circ}$ (for this case) J_{hkl} is equal to 712.83 for the 121 θ data. To test the accuracy of these data a new value of J_{hkl} was calculated with $\Delta\alpha = 3^{\circ}$ and $\Delta\beta = 10^{\circ}$. The new J_{hkl} was equal to 624.40. If all the corrected intensities are divided by this factor it will be observed that the "times random" units levels are increased by 12.4%, that is the texture appears slightly sharper. This is the only significant change that could occur if $\Delta\alpha$ is smaller, the crystallographic relationships remaining unaffected.

Finally it was observed that the $(\bar{1}\bar{1}1)$ pole in the {111}K pole figure could be moved to the center and if a transmission Laue photograph of the specimen was taken in that orientation a three fold symmetry should appear. The necessary rotations were measured in the pole figure and estimated to be 16° down and 20° to the left. Figure 20b is such a photograph obtained with CuK$_\alpha$ radiation. As was expected the three fold symmetry is present, the planes reflected being the {200}K. The actual rotations of the specimen were 14° down and 23° to the left. The same test was repeated, this time using W radiation and the results are shown in Figure 21. Here the symmetry is due to the {333}K planes.

VI. DISCUSSION

As has been pointed out by other investigators (11, 12, 25, 27, 28) the Al-CuAl$_2$ eutectic system is not a simple one. The structure of the θ phase is very complex, the lamellae usually will show all the defects associated with this type of microstructure (Figs. 4 and 5) and the interfacial structure is also irregular and imperfect (30). But in spite of all these complexities the crystallographic relationships between the phases seem to remain fairly constant if we do not consider the disagreements existing with respect to the habit plane.

This work has verified the existence of the interfacial relationship {111}K || {121}θ. Kraft (25) used an indirect method to arrive at a similar general result by constructing an idealized stereogram obtained from x-ray data. The electron microscope investigations as listed in Table 1 show that this relationship has also been found but it is always reported in the same general form. In this experiment it was possible

to find a definite crystallographic relationship by directly recording the peak profiles of the reflections coming from the two interfacial planes. This finding allows us to make two statements in an attempt to explain the discrepancies associated with the lamellar plane:

a) By examining Fig. 18 another relationship can be found: $(1\bar{1}1)K||(2\bar{1}1)\theta$ but now the two planes are separated by about 18°. The discrepancy can be due to the consideration of this set of planes which is separated from the $(111)K||(21\bar{1})\theta$ set by less than 78°.

b) It will be necessary to further explore the crystallographic variation of the two specific planes reported here when the growth conditions are changed. If the relationship varies, the discrepancies are due to kinetic factors and if no change is observed, it can be concluded that the crystallographic relationships for the $Al-CuAl_2$ eutectic are invariable.

APPENDIX A

RECORDING X-RAY DATA

Installing and Setting the Instrument to Zero:

a) Install a Cu x-ray tube, Ni filter. Collimation slits: 1°, MR, 0.3°. If any other combination of slits is found more convenient to use do so, but be consistent and maintain the same arrangement throughout the entire experiment.

b) Assemble the instrument as illustrated in Fig. 6b. Mount it in the diffractometer. Secure the base to the diffractometer table with four screws. Sometimes it is convenient to skip this last step, especially when aligning the instrument. If this step is omitted make sure that the base is firmly attached to the diffractometer table and that there is not lateral play between the base and the table.

c) Place a round piece of fluorescent material in the center hole of specimen holder No. 1 (Fig. 7). Secure it from the back using scotch tape or plasticine. Mount holder in the appropriate location in the instrument.

d) Lightly unscrew knob A and set screw C. Manually move the diffractometer table to the zero position. Turn knob B and move slide D until the front surface of the specimen holder lies in the same straight line joining the center of the x-ray source slit and the center of the detector slit.

e) Remove the protective cover from the diffractometer axis and place a lead shield between you and the diffracted beam. Set the voltage at about

10 Kv and the current at about 5 Ma. Turn x-ray source on and observe

at what point the x-ray beam is visible on the fluorescent material. If

the beam is not exactly at the center of the hole in the specimen holder,

move slide D to the back or to the front as needed.

Caution: Remember to turn x-ray source off before making any

adjustment to the instrument.

f) Remove holder from the instrument and replace the ZnS piece with the

LiF single crystal in a similar way as the fluorescent piece. The flat

side must be horizontal. Reinstall protective cover in the diffractometer

holder area.

g) Turn x-ray source on. Turn chart recorder on. CuK_α should appear

at $2\theta = 44.95^\circ$. Move slide D by very small distances until a maximum

intensity of the CuK_α peak is obtained at a value of 2θ close to the

desired value. Usually a combination of motions (turning the knob B and

moving the slide D) is needed to get a maximum intensity at a value of

$2\theta = 44.95^\circ$.

h) Loosen ring E by a few turns and set graduated disk F at zero.

Tighten ring E and knob A. Screw set screw C fixing the slide at this

position. Remove specimen holder.

j) Install holder $N^\circ 2$. Mount eutectic specimen as shown in Fig. 7. Be

sure that the sample is located at the center of the hole in the specimen

holder. If this is not correct, the background intensity will vary with

β which in turn gives unreliable data. The specimen must be suspended up

in the air, the x-ray beam should impinge only on the sample and not on

any part of the specimen holder. Reflected x-ray radiation from the holder

also alters the background. Hold the eutectic specimen with plasticine from the back, not from the sides. Plasticine gives a high intensity peak at a 2 θ value very close to the {121} θ reflections.

k) Turn on the x-ray source. Use settings already mentioned under EXPERIMENTAL. Scan from 2 θ = 20° to 2 θ = 140°. Identify the reflections obtained. Do this for the three mutually perpendicular faces of the specimen (Table 2).

Data for the Pole Figures

a) Mount the specimen with the transverse side facing the x-ray source. Let the diffractometer table scan from about 2θ = 35° to 2θ = 41° recording the peaks and the background intensities. Start with β = 0° positioning needle H at the point marked 90° on dial K. Tighten screw G firmly every time you change the setting of β and also tighten knob A whenever the value of α is changed. β should be kept at zero while takes on values from +18° to -18°. Take readings at α = 0, 6, 12, 18 plus some values in between getting enough points to allow you to draw the correction curve using the background radiation shown in Fig. 10.

b) Take readings scanning from 2θ = 36.50° to 2θ = 40° at α = 0° changing β by increments of 10°. Start at β = +90° (0° in dial K) and go down to β = -90. This same operation will be repeated later when CrK_α radiation is used to cover the blind region of the pole figure. A correlation must be found between the two data for each value of β when α = 0°. This correlation is needed to convert CrK_α intensities to CuK_α values.

c) Now you are ready to start recording the rest of the data. Start at $\beta = 90^\circ$, $\alpha = 18^\circ$. Keep β fixed, vary α by 6°. Sometimes you will not get any information at $\alpha = 18^\circ$ due to the specimen holder interferring with the x-ray beam. This part of the data can be obtained later when covering the blind region with CrK_α radiation. Remember that $\Delta\beta = 10^\circ$, therefore after finishing the run for $\beta = 90^\circ$ go to $\beta = 80^\circ$, fix it at this setting and as before start with $\alpha = 18^\circ$ decreasing it in increments of 6° ($\Delta\alpha = 6^\circ$). Your recorded data should look like that of Fig. 9.

Covering the Blind Region

It is known that even with an ideal specimen holder data can be obtained in reflection only up to $\alpha = \theta$. After that it is necessary to take measurements in transmission. Also there is a blind region caused by the specimen holder retainer parts and other necessary appendages. This blind region covers a range of about $\alpha = \theta - 10$ to $\alpha = \theta + 10$.

This region is spanned by changing x-ray tubes. The Cu tube is replaced with a Cr tube and the same alignment procedure must be repeated using a V filter. Repeat part b of data for the Pole Figures and verify that the trend observed then is also followed here. Record the background intensities keeping $\beta = 0$ and changing α as it was done on part a. Again obtain as many points as necessary to draw another correction curve for absorption. Start at $\alpha = 24^\circ$ now. λ for Cr is equal to 2.29 A$^\circ$, therefore the (111) peak should appear at $2\theta = 58.55^\circ$. Scan from about 57° to 61°. Repeat part c, but now $\alpha = 24, 18, -18, -24$ ($\alpha = 0$ was already recorded at the beginning).

Transmission Data

a) Mount the instrument as illustrated in Fig. 6c. Remove the Cr tube
and install back the Cu tube. Repeat alignment procedure. Cut your
transmission sample as explained under Experimental.. Mount the trans-
mission specimen. The side that was facing the x-ray beam in reflection
should be in the same position now. Hold the specimen in place with a
piece of electric or scotch tape.

b) Start at $\alpha = 90^{\circ}$, $\beta = 90^{\circ}$. Follow the same steps as before, i.e.,
$\Delta\alpha = 6^{\circ}$, β fixed. Change β by 10°, etc. Remember now you have to go
from $\alpha = 90^{\circ}$ to $\alpha = 30^{\circ}$ and from $\alpha = -30^{\circ}$ to $\alpha = -90^{\circ}$.

APPENDIX B

TEXTURE

Texture or preferred orientation can be defined as a condition in which the distribution of crystal orientations in a polycrystalline aggregate is nonrandom (41). Two kinds of texture should be distinguished: deformation texture which results from the nonrandom arrangement of crystallites in a mechanically worked material (cold drawn wire or cold rolled sheet) and orientation texture, an intrinsic property of the polycrystalline material which reflects its mode of growth as in castings, electrodeposited layers, eutectic alloys, etc. (46).

Preferred orientation is detected when a pinhole photograph is made of a polycrystalline specimen using characteristic x-ray radiation. If preferred orientation is not present, the Debye rings observed are of uniform intensity all around their circumference. If there is preferred orientation the Debye rings will be discontinuous (Fig. 20), the discontinuities arising because the orientations which would reflect to those parts of the ring are not present in the specimen. Nonuniform Debye rings can therefore be taken as a definite evidence for the existence of preferred orientation (41, 42).

Texture can best be described by means of a pole figure, which is a stereographic projection showing the variation in pole density with pole orientation for a selected set of low index crystal planes. The earliest method of evaluating preferred orientation consisted in taking a series of transmission photographs of the specimen at different angles in order to obtain the information needed to construct the pole figure (42).

Presently the most common procedure is to use x-ray texture goniometry to determine a pole figure.

When using the x-ray Geiger-Counter spectrometer to determine quantitative pole figures a combined transmission-reflection method is used (47, 49). Transmission techniques provide the data for the outer regions of the pole figure and the reflection techniques give the central part; both techniques are limited by geometrical considerations (43).

<div align="center">

Quantitative Determination of
Preferred Orientation

</div>

When data for a complete pole figure is needed, different problems arise which usually prevent accurate determination of the preferred orientation. Corrections for angle dependent absorption are required and in many cases it is found that a blind region exists where data can not be obtained. Bragg and Packer (45) derived formulas to make the absorption corrections and showed that these correction factors can be obtained directly from measurements of the background radiation (Fig. 10). They also solved the problem of spanning the blind region (37) by suggesting two methods to accomplish this. One consisted in using a higher order of the same reflection and the other in changing the x-ray tube. In both cases it is necessary to calculate the ratio of the two intensities obtained to convert from one set of data to the other (see data analysis).

Dunn analyzed the quantitative pole figure data visualizing the pole density as a height above a plane that lies in the surface of the stereographic projection reference sphere and the distribution of pole density

as a surface above this plane. This surface is a bivariate frequency surface. If the pole figure consists of a sharp single-orientation texture, the bivariate surface for an isolated concentration of poles may take the form of a normal distribution function (48).

Bragg and Packer (37) showed that the results obtained by Dunn are of general applicability. In the Bragg and Packer method the orientation distribution $p(\alpha, \beta)$ is defined in units of "times random" and is unity for a random specimen. α is the angle which measures the amount of rotation about the diffractometer axis and $\alpha = 0$, at the exact para-focussing condition. β is the angle by which the specimen can be rotated in its own plane away from some reference position $\beta = 0$.

The integrated intensity for a random specimen is given by:

$$J_{hkl} = I_o (e^2/m^*c^2)^2 \frac{\lambda^3 (1 + \cos^2 2\theta)}{v^2 \sin^2 \theta \cos\theta} m F_{hkl}^2 \delta V \qquad \text{(Eq. 10)}$$

The quantity sought for the pole figure is:

$$p(\alpha, \beta) = I_{hkl}(\alpha, \beta)/J_{hkl}.A(\theta, \alpha) \qquad \text{(Eq. 11)}$$

where $I_{hkl}(\alpha, \beta)$ is the integrated intensity for a given specimen orientation (α, β) and $A(\theta, \alpha)$ is the absorption factor. Equation 11 shows that when the observed intensities are corrected for absorption the resulting intensities are converted to "times random" by dividing by J_{hkl}. To calculate J_{hkl} equation 12 is obtained from equation 11 after a few mathematical manipulations

$$J_{hkl} = \frac{\Delta\alpha\Delta\beta}{2\pi} \sum_{\alpha} \sum_{\beta} \frac{I_{hkl}}{A(\theta,\alpha)} \sin \alpha \qquad\qquad \text{(Eq. 12)}$$

This result indicates that J_{hkl} can be easily calculated from the experimental data by performing a double summation over the corrected intensities weighted by the factor $\sin \alpha$.

REFERENCES

1. G. H. May and D. P. H. Jones, The Production and Properties of Directionally Solidified Composites, Metals and Materials, 8, 242-244 (April 1974).

2. F. D. Lemkey and E. R. Thompson, Met. Trans. 2, 1537 (1971).

3. H. Weiss, Met. Trans. 2, 1513 (1971).

4. J. May, Directional Solidification: A New Route for Eutectic Alloys in Tough Applications, Metals and Materials, 44-48 (September 1975).

5. L. M. Hogan, R. W. Kraft and F. D. Lemkey, Advances in Materials Research, 5, 83 (1971).

6. W. Rosenhain and P. A. Tucker, Eutectic Research, No. 1, The Alloys of Lead and Tin, Ph. Trans. Roy. Soc., Ser. A, 209, 89 (1909) Reference 26 of 5.

7. M. Straumanis and N. Brakss, The Structure of the Bi-Cd, Sn-Zn, Sn-Cd and Al-Si Eutectics, Z. Phys. Chem., B 38-39, 140 (1937-38) Reference 16 of 5.

8. H. W. Weart and D. J. Mack, Eutectic Solidification Structures, Trans. Met. Soc. AIME 212, 664 (1958).

9. R. W. Kraft and D. L. Albright, Crystallographic Substructures of Lamellar $Al-CuAl_2$ Eutectic, Trans. Met. Soc. AIME 224, 1176 (1962).

10. D. D. Double and A. Hellawell, Lattice Rotations in Eutectic Crystals, Phil. Mag. 19, 1299 (1969).

11. I. G. Davies and A. Hellawell, Phase Orientations in the Lamellar and Non-lamellar Regions of the $Al-CuAl_2$ Eutectic Alloy, Phil. Mag. 20, 1255 (1970).

12. B. Cantor and G. A. Chadwick: The Growth Crystallography of Uni-directionally Solidified Al-Al$_3$Ni and Al-Al$_2$Cu Eutectics, Journal of Crystal Growth, 23, 12-20 (1974).

13. A. L. Ruoff, Introduction to Materials Science, Prentice-Hall, Inc. Englewood Cliffs, New Jersey (1972).

14. L. J. Salmon, Experimental Techniques for Growing Unidirectionally Solidified Oriented Eutectics, M. S. Thesis, University of California, Berkeley, June 1973.

15. B. Chalmers, Principles of Solidification, John Wiley and Sons, Inc., New York (1964).

16. E. Scheil, On Eutectic Crystallization, Giesserei 24, 1313 (1959). Reference 8 of 5.

17. P. G. Shewmon, Transformation in Metals, McGraw-Hill Inc., New York (1969).

18. W. A. Tiller, "Polyphase Solidification" in Liquid Metals and Solidification, ASM, Cleveland, Ohio (1958). Reference 34 of 5.

19. W. D. Winegard, S. Majka, B. M. Thall, and B. Chalmers, Can. J. of Chem, 29 320 (1957). Reference 16 of 15.

20. D. Turnbull, "Principles of Solidification" from Thermodynamics in Physical Metallurgy, published by the ASM, Cleveland, Ohio (1949).

21. K. Jackson and J. D. Hunt, Lamellar and Rod Eutectic Growth, Trans. Met. Soc. AIME. 236, 1179 (1966).

22. B. Chalmers, Melting and Freezing, Institute of Metals Lecture, Trans. AIME 200, 519 (1954).

23. R. W. Kraft and D. L. Albright, Microstructure of Unidirectionally Solidified Al-CuAl$_2$ Eutectic, Trans. Met. Soc. AIME 221, 95 (1961.

24. G. A. Chadwick, Solidification of CuAl$_2$-Al Eutectic Alloys, Journal of the Institute of Metals, 91, 169 (1963).

25. R. W. Kraft, Crystallography of Equilibrium Phase Interfaces in Al-CuAl$_2$ Eutectic Alloys, Trans. Met. Soc. AIME, 224, 65 (1962).

26. E. C. Elwood and K. Q. Bagley, The Structure of Eutectics, J. Inst. of Metals, 76, 631 (1949).

27. R. W. Kraft, Technique for Determining Orientation Relationship and Interfacial Planes in Polyphase Alloys: Application to Controlled Eutectic Specimen, Trans. Met. Soc. AIME, 222, 704 (1961).

28. I. G. Davies and A. Hellawell, The Structure of Directionally Frozen Al-CuAl$_2$ Eutectic Alloy, Phil. Mag. 19, 1285 (1969).

29. N. Takahashi, Electron Microscopy Study of Thin Films of the Aluminum-Copper Eutectic Prepared by a Melting Method, Journal of Applied Physics, 31, 1287 (1960).

30. G. Garmong and C. G. Rhodes, Interfacial Structure of Al-CuAl$_2$ Eutectic Composites, Acta. Met., 22, 1373 (1974).

31. M. Dupeux and F. Durand, Anisotropic Tensile Properties of Lamellar Al-CuAl$_2$ Eutectic Composite, Met. Trans. 6A, 2143 (1975).

32. E. Ho and G. C. Weatherly, Interface Diffusion in the Al-CuAl$_2$ Eutectic, Acta. Met., 23, 1451 (1975).

33. E. Scheil, "Eutectic Crystallization", Z. Metallk., 45, 298, (1954) Reference 21 of 5.

34. C. Zener, Kinetics of the Decomposition of Austenite, Trans. AIME, 167, 550 (1946).

35. W. H. Brandt, Some Factors Affecting Edgewise Growth of Pearlite, Trans AIME, 167, 405 (1946).

36. M. Hillert, Jernkontorets Ann. 144, 520 (1960). Reference 4 of 21.

37. R. H. Bragg and C. M. Packer, Quantitative Determination of Preferred Orientation, J. Appl. Phys. 35 (4), 1322 (1964).

38. W. T. Read and W. Shockley, Dislocation Models of Crystal Grain Boundaries, Phys. Review, 78, 275 (1950).

39. D. D. Double, P. Truelove and A. Hellawell, J. Crystal Growth, 2, 191 (1968).

40. L. D. Graham and R. W. Kraft, Coarsening of Eutectic Microstructures at Elevated Temperatures, Trans. Met. Soc. AIME, 236, 94 (1966).

41. B. D. Cullity, Elements of X-ray Diffraction, Addison-Wesley Publishing Co., Reading Massachusetts, (1967).

42. C. S. Barret and T. B. Massalski, Structure of Metals, McGraw-Hill Book Company, New York (1966).

43. A. H. Geisler, Modern Research Techniques in Physical Metallurgy, ASM, Cleveland, p.131, _(1953).

44. G. J. Davies, JOM p. 21-28 (July 1976).

45. R. H. Bragg and C. M. Packer, The Review of Scientific Instruments, 34,(11), 1202 (1963)

46. L. V. Azaroff, Elements of X-ray Crystallography, McGraw-Hill Book Co., New York (1968).

47. B.F. Decker, E. T. Asp and D. Harker, J. Appl. Phys. 19, 338 (1948).

48. C.G. Dunn, J. Appl. Phys. 25, 233 (1954)

49. M. Field, M. E. Merchantt, J. Appl. Phys. 20, 741 (1949).

TABLE 1

Crystallographic Data for the Al-CuAl$_2$ Eutectic

Investigator, method used and specimen preparation	Orientation Relationships		
	Between Phases	Interfacial	Growth Direction
E.J. Elwood and K.Q. Bagley (26). X-ray technique. Wires drawn up from liquid alloy and passed through a gradient furnace. Cooling rate: 60°C/hr.	(001)Al||(001)θ [100]Al||[100]θ		(001) axis of θ perpendicular to the temperature gradient.
Noboru Takahashi (29) Electron microscopy spot pattern analysis Thin films prepared in air by dipping a small loop of iron wire into molten bath and withdrawing it at a rate of 2 cm/s	(001)Al||(001)θ [110]Al||[100]θ		Not reported
R.W. Kraft (27). X-ray specially designed back reflection camera. Specimens taken from unidirectionally solidified ingots at a rate of 9.8 cm/hr.	(001)Al≃||(001)θ [210]Al≃||[100]θ	(1̄1̄1)Al||(2̄2̄1)θ	(112)Al and (102)θ low index planes closest to being parallel to solid/liquid interface.
R.W. Kraft (25).Same technique as above. Data obtained from several slowly grown eutectic. Growth rate not reported.		{111}Al||{211}θ <101>Al||<210>θ	Parallel to [1̄12]Al

TABLE 1. continued

Investigator, method used and specimen preparation	Orientation Relationships		
	Between Phases	Interfacial	Growth Direction
I.G. Davies and A. Hellawell (11). Electron microscopy spot pattern analysis. Specimens grown in graphite tubes, unidirectionally solidified. Temperature gradient 50°C/cm Growth Rate 0.36 cm/hr. Material cooled in the solid state at a mean rate of 0.25° C/min.		$\{111\}Al\|\|\{211\}\theta$ $<110>Al\|\|<210>\theta$ Interface habit plane 12° away of $\{111\}Al$, $\{211\}\theta$	Growth axis approximately $[\bar{2}11]Al$
B. Cantor and G.A. Chadwick (12). Electron microscopy Kikuchi line electron diffraction techniques. Single crystals grown by a melt back method. Growth rate 4 cm/hr.		$\{111\}Al\|\|\{211\}\theta$ $<110>Al\|\|<210>\theta$ Interface facets within 8° from $\{111\}Al$, $\{211\}$	Varied. It was usually between $\{321\}Al$, $\{211\}Al$ and $\{310\}Al$

TABLE 2

X-ray Diffractometer Reflection Data. Al-CuAl$_2$ Eutectic
Sample. Cu Radiation, Ni Filter, 40 Kv, 20 ma.
Range 500, Intensities in Arbitrary Units.

FACE	PEAK No	d (A°)	2⊖ (deg)	(hkl)⊖	(hkl)K	Intensity
TOP	1	2.370	37.90	121		500+
	2	1.170	81.90	114		135
	3	.957	107.00	532, 620		100
	4	.905	116.40	424	420	500+
LONGITUDINAL	5	2.340	38.40		111	465
	6	2.020	44.67		200	185
	7	1.070	92.02	152		300
	8	.810	144.22	444		315
TRANSVERSE	10	2.340	38.40		111	380
	11	2.046	44.20		200	180
	12	1.430	65.20	330	220	110
	13	1.030	97.02	350, 134		315
	14	.905	116.40	424	420	500+

TABLE 3

Correction Factors

A. Peak Interference

PEAK RATIOS	θ	1	3/4	1/2	1/3	1/4	1/6
	K	1	1	1	1	1	1
FACTOR	θ	.94	.96	.77	.76	.73	.69
	K	.94	.94	.96	.97	.99	.99

B. Geometric

$\beta°$	0	10	20	30	40	50	60	70	80	90
FACTOR	1.00	.982	.932	.916	.965	.982	1.06	1.12	1.20	1.22

C. Absorption Factors

$\alpha°$	-18	-12	-6	0	6	12	18
REFLECTION	2.20	1.61	1.30	1.00	.698	.390	.067

$\alpha°$	30	36	42	48	54	60	66	72	78	84	90
TRANSMISSION	.223	.374	.510	.619	.707	.776	.834	.881	.924	.963	1.00

TABLE 4
Some Selected Values of α(degrees) at Constant β.
{111}K Phase

| | Intensity Levels ("times random" units) | | | | | | | | | | | | | | |
| | 0.50 | | | 1.00 | | | 2.50 | | | 9.00 | | | 12.00 | | |
β°	L	C	R	L	C	R	L	C	R	L	C	R	L	C	R
90	-57	18	0	-56	4	0	-54	0	0	0	0	0			
	-47	18	0	-48	16	0	-52	0	0	0	0	0			
70	-63	-4	65	-56	7	0	0	0	0	0	0	0			
	-52	21	68	-56	13	0	0	0	0	0	0	0			
50	-89	-6	62	0	0	0	0	10	0	0	20	0	0	23	0
	-50	37	68	0	34	0	0	30	0	0	25	0	0	23	0
40	0	-4	85	0	3	87	0	12	0	0	20	0	0	22	0
	0	41	→	0	37	0	0	33	0	0	28	0	0	25	0
20	←	-4	79	←	3	81	←	12	84	←	0	87	0	0	89
	-83	36	→	-84	28	→	-85	21	→	-89	0	→	0	0	→
0	0	-6	0	0	5	0	0	0	0						
	0	27	0	0	16	0	0	0	0						
-10	0	-4	0	0	0	0									
	0	23	0	0	0	0									
-60	-69	-4	37	-66	0	38	0	0	43	0	0	0			
	-64	8	47	-66	0	45	0	0	43	0	0	0			

L: Left curve of the graph
C: Center curve
R: Right curve
An arrow indicates that α >|90°|

TABLE 5

Angles Between Planes of the Form {121} for the θ Phase. Tetragonal System.

	121	1̄21	12̄1	121̄	1̄2̄1	1̄21̄	12̄1̄	1̄2̄1̄
121	0	46.00	102.80	58.19	121.80	77.19	134.00	180.00
1̄21	46.00	0	121.80	77.19	102.80	58.19	180.00	134.00
12̄1	102.80	121.80	0	134.00	46.00	180.00	58.19	77.19
121̄	58.19	77.19	134.00	0	180.00	46.00	102.80	121.80
1̄2̄1	121.80	102.80	46.00	180.00	0	134.00	77.19	58.19
1̄21̄	77.19	58.19	180.00	46.00	134.00	0	121.80	102.80
12̄1̄	134.00	180.00	58.19	102.80	77.19	121.80	0	46.00
1̄2̄1̄	180.00	134.00	77.19	121.80	58.19	102.80	46.00	0
211	32.08	76.31	76.31	68.02	111.97	103.68	103.68	147.91
2̄11	76.31	32.08	76.31	103.68	76.31	68.02	147.91	103.68
21̄1	76.31	111.97	32.08	103.68	76.31	103.68	68.02	103.68
211̄	68.02	103.68	103.68	32.08	147.91	76.31	76.31	111.97
2̄1̄1	111.97	76.31	76.31	147.91	32.08	103.68	103.68	68.02
2̄11̄	103.68	68.02	147.91	76.31	103.68	32.08	111.97	76.31
21̄1̄	103.68	147.91	68.02	76.31	103.68	111.97	32.08	76.31
2̄1̄1̄	147.91	103.68	103.68	111.97	68.02	76.31	76.31	32.08

	211	2̄11	21̄1	211̄	2̄1̄1	2̄11̄	21̄1̄	2̄1̄1̄
211	0	102.80	46.00	58.19	121.80	134.00	77.19	180.00
2̄11	102.80	0	121.80	134.00	46.00	58.19	180.00	77.19
21̄1	46.00	121.80	0	77.19	102.80	180.00	58.19	134.00
211̄	58.19	134.00	77.19	0	180.00	102.80	46.00	121.80
2̄1̄1	121.80	46.00	102.80	180.00	0	77.19	134.00	58.19
2̄11̄	134.00	58.19	180.00	102.80	77.19	0	121.80	46.00
21̄1̄	77.19	180.00	58.19	46.00	134.00	121.80	0	102.80
2̄1̄1̄	180.00	77.19	134.00	121.80	58.19	46.00	102.80	0

TABLE 6

Measured Angles Between Poles (degrees).

θ Phase Pole Figure.

	121	$\bar{1}21$	$21\bar{1}$	$\bar{2}11$	$\bar{2}\bar{1}1$
121	0	43	68	78	114
$\bar{1}21$	43	0	103	112	78
$21\bar{1}$	68	103	0	78	175
$\bar{2}11$	78	112	78	0	100
$\bar{2}\bar{1}1$	114	78	175	100	0

TABLE 7

Angles Between Planes of the Form {111}

for the Cubic System (degrees).

	$\bar{1}\bar{1}1$	$\bar{1}11$	111	$1\bar{1}1$	$\bar{1}\bar{1}\bar{1}$
$\bar{1}\bar{1}1$	0	70.52	109.47	70.52	70.52
$\bar{1}11$	70.52	0	70.52	109.47	109.47
111	109.72	70.52	0	70.52	180.00
$1\bar{1}1$	70.52	109.47	70.52	0	109.47
$\bar{1}\bar{1}\bar{1}$	70.52	109.47	180.00	109.47	0

FIGURE CAPTIONS

Fig. 1. Optical micrograph of a directionally solidified Al-CuAl$_2$ eutectic (side view). G = 44°C/cm, R = 25.6 m/s, magnification 600x. (a) a single grain. (b) two grain microstructure.

Fig. 2. Al-Cu pseudobinary phase diagram.

Fig. 3. (a) Scale model of the θ phase unit cell (body centered tetragonal). (b) The θ unit cell oriented with the (211) plane horizontal. (c) Scale model of the K phase unit cell (face centered cubic). (d) Illustration of the interfacial relationship (111)K (211)θ. (e) The two scale models placed together for comparison.

Fig. 4. Optical micrographs of the directionally solidified Al-CuAl$_2$ eutectic grain used in this work.

Fig. 5. Sketch of the eutectic grain drawn from the micrographs of figure 4.

Fig. 6. (a) Original x-ray texture instrument. (b) Modified instrument used in reflection. (c) Modified instrument as it was used in transmission. (d) Transmission set up. Instrument mounted in the diffractometer.

Fig. 7. (a) Specimen holder number 1, used for the instrument alignment. (b) Fluorescent material (ZnS). (c) LiF single crystal. (d) Specimen holder used in reflection showing the specimen as it was held in place. Scale 2:1.

Fig. 8. The G. E. XRD-3 equipment used showing the actual recording of the data.

Fig. 9. A typical set of data showing the {111}K peak and the {121}θ peak merging into one when α = -12°.

Fig. 10. The same set of Figure 9 after the peak profiles had been drawn.

Fig. 11. (a) and (b) resultant curves obtained from the interaction of two components, in this case the {111}K and {121}θ peaks which are separated by 0.45°.

Fig. 12. Geometrical representation of the variation in the diffracted area when β varies from 0° to 90°.

Fig. 13. (a) Plot of "Times random" units vs α at a fixed β. {111}K, β = 60°. (b) Same as (a), β = -30°.

Fig. 14. Standard cubic (112) stereographic projection including only the {111} poles.

Fig. 15. {111}K pole figure.

Fig. 16. {121}θ pole figure.

Fig. 17. The two pole figures superimposed.

Fig. 18. Results obtained when the two pole figures are superimposed.

Fig. 19. Trace analysis to determine approximate growth direction of the lamellae.

Fig. 20. Transmission x-ray pinhole photographs of the specimen of Fig. 4. Cu radiation, 45 Kv, 20 ma, specimen to film distance 3.0 cm. (a) as grown orientation. (b) [$\bar{1}\bar{1}$1] orientation.

Fig. 21. Same as Fig. 20. W radiation, 45 Kv, 20 ma, specimen to film distance 4.5 cm. (a) as grown orientation. (b) [$\bar{1}\bar{1}$1] orientation.

growth direction
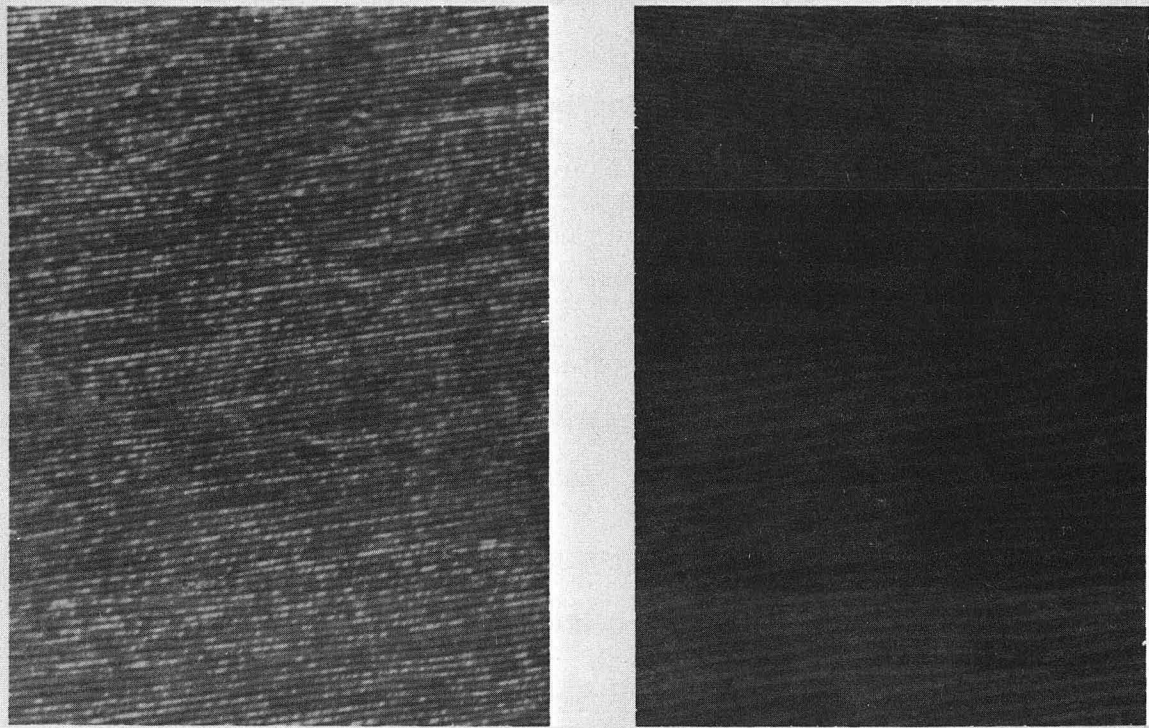
XBB 773-1909

25 μ

Fig. 1
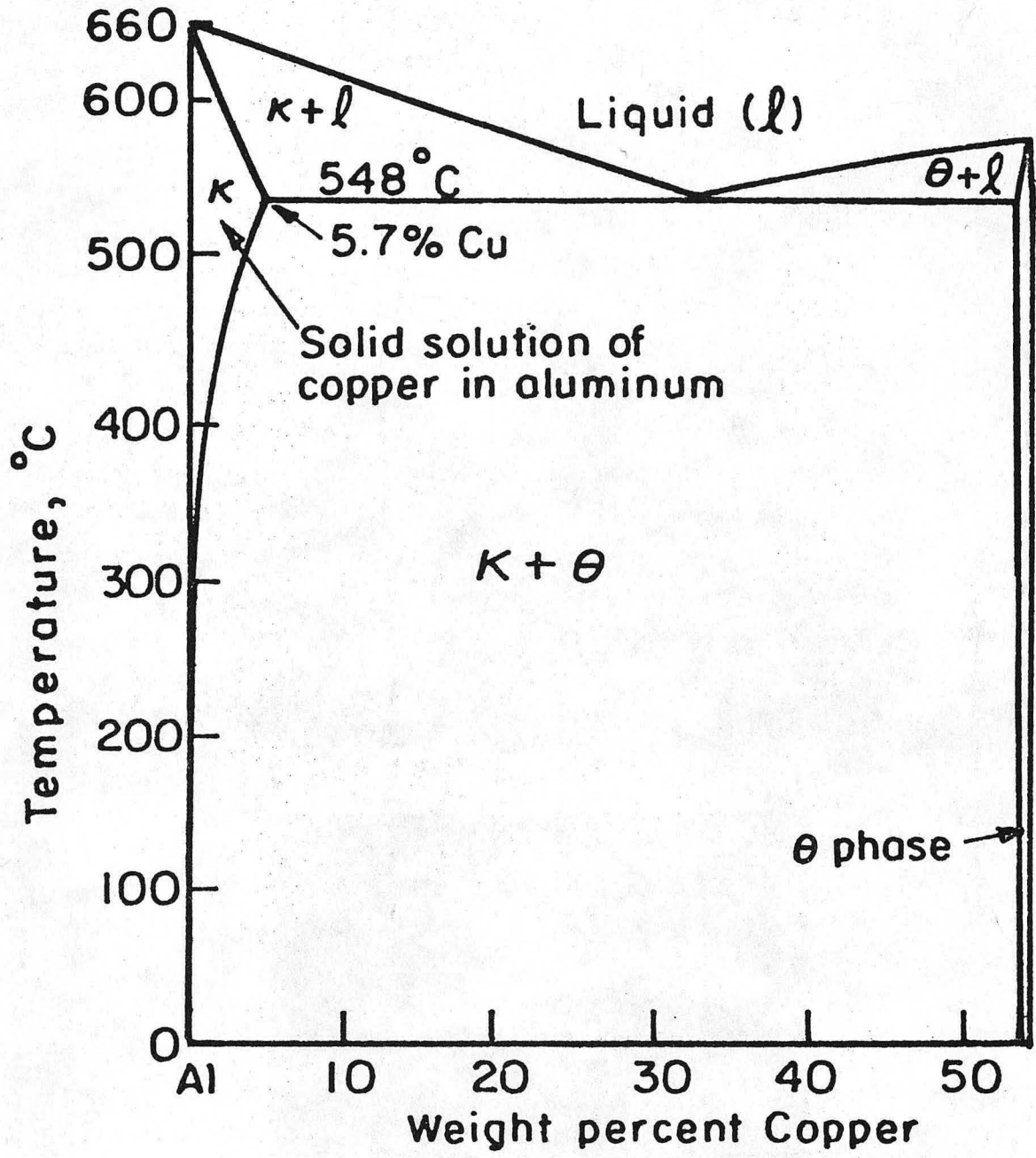
FIG. 2

XBL 7412-7840
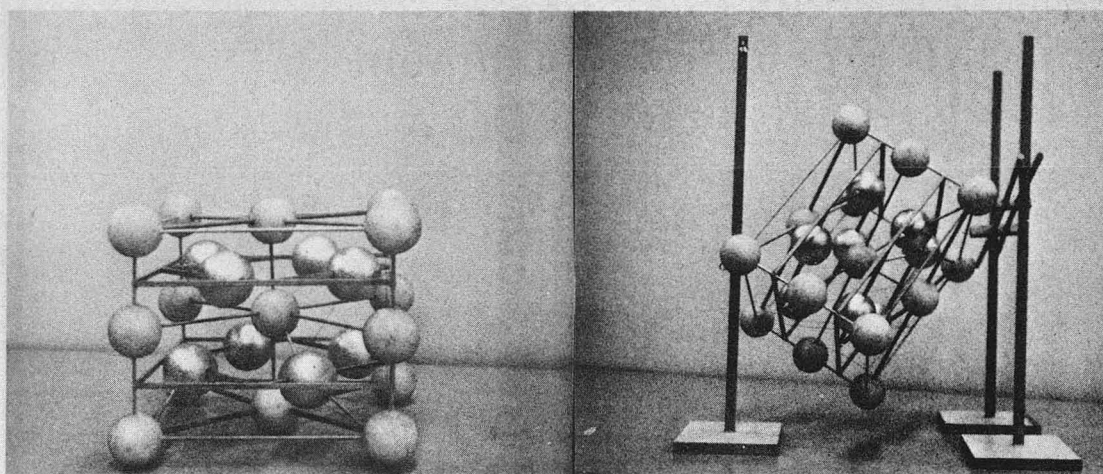
(a)

(b)
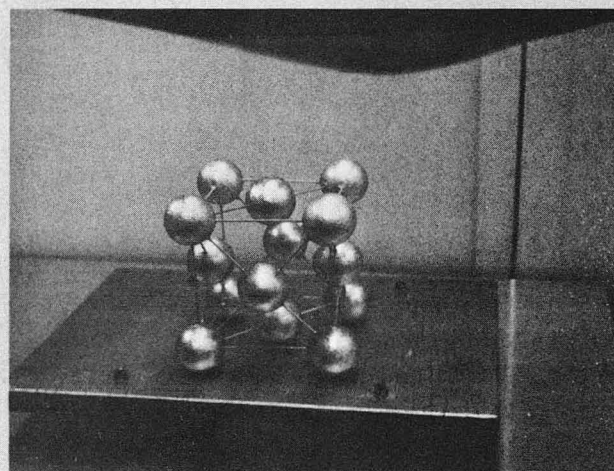
(c)   XBB 773-1907

Fig. 3
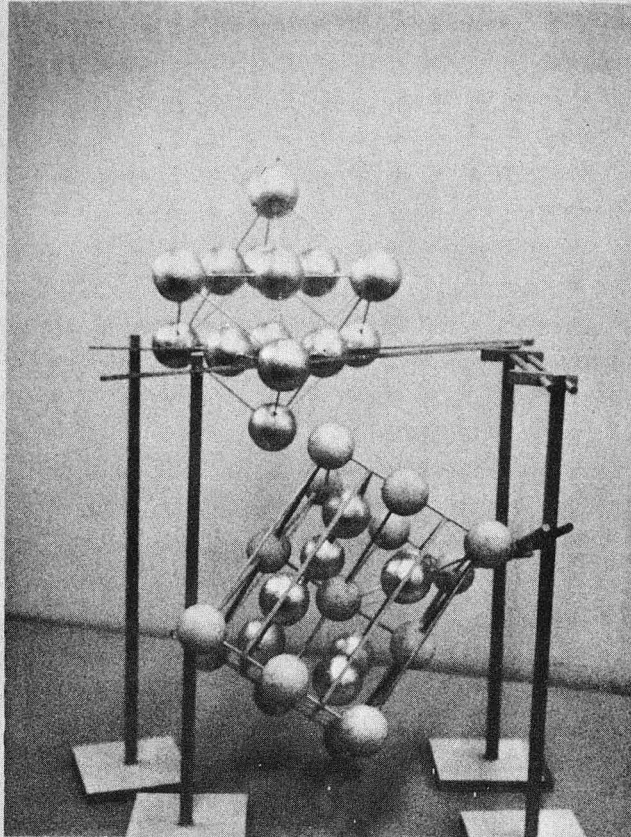
(d)
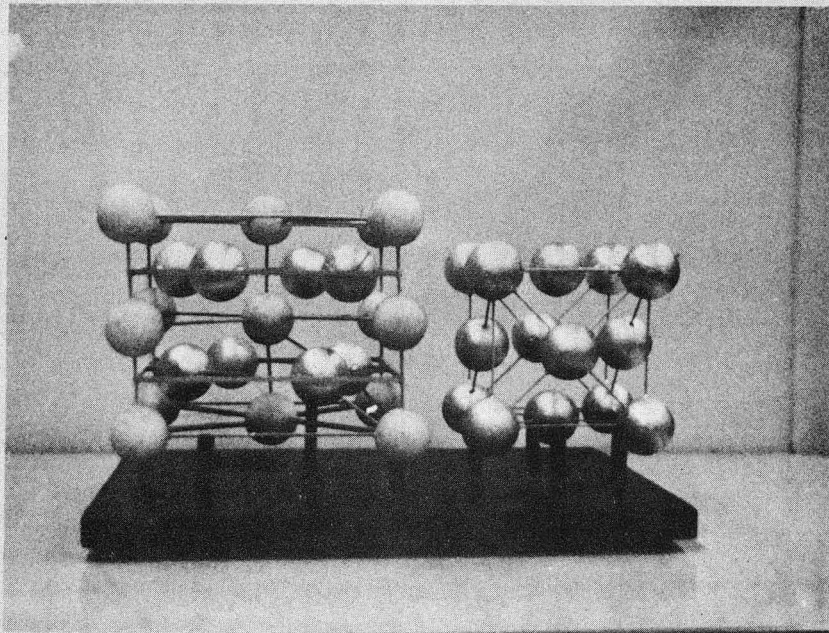
(e)   XBB 773-1908

Fig. 3

Top view
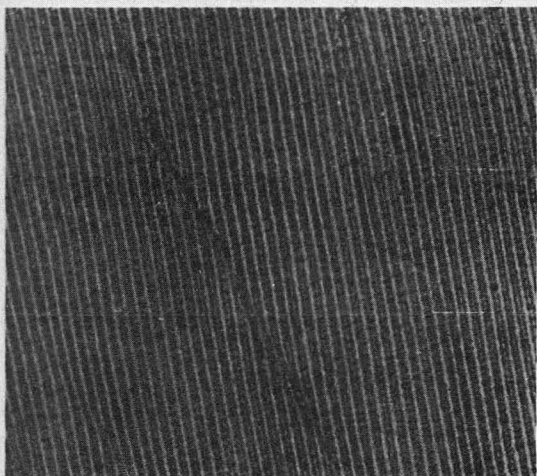
growth direction

Transverse

Longitudinal

25 μ
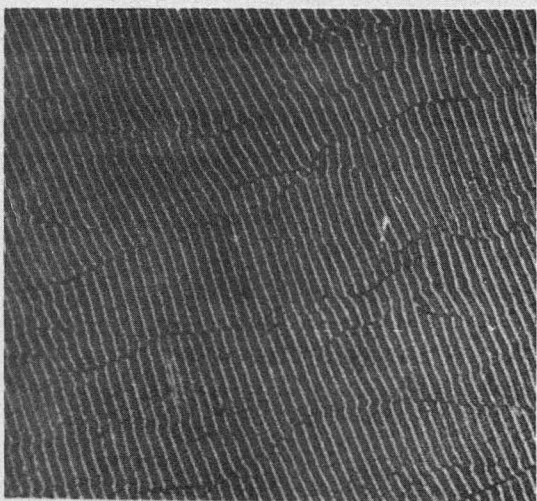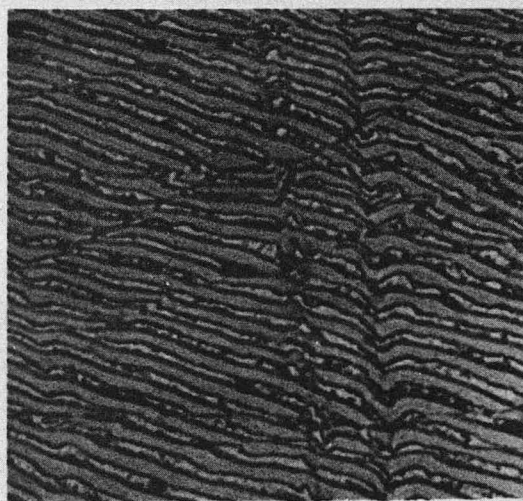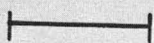
growth direction

XBB 770-13050

Fig. 4

TRANSVERSE
DIRECTION

17.5°

90°

19°

GROWTH DIRECTION
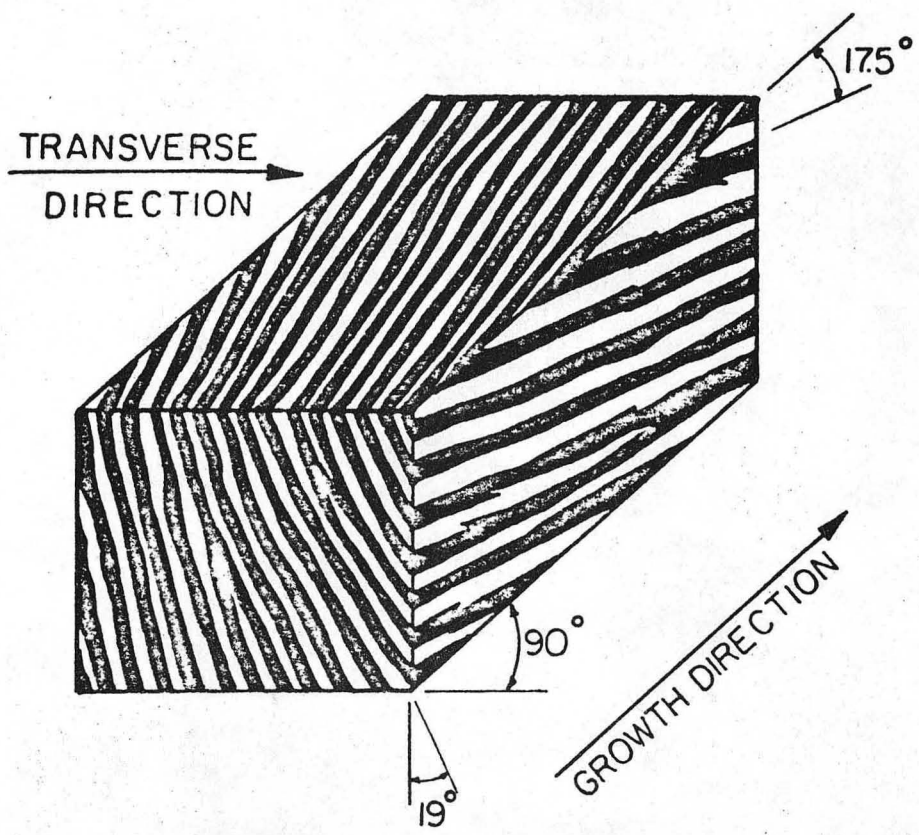
XBL 7712-6592

FIG. 5
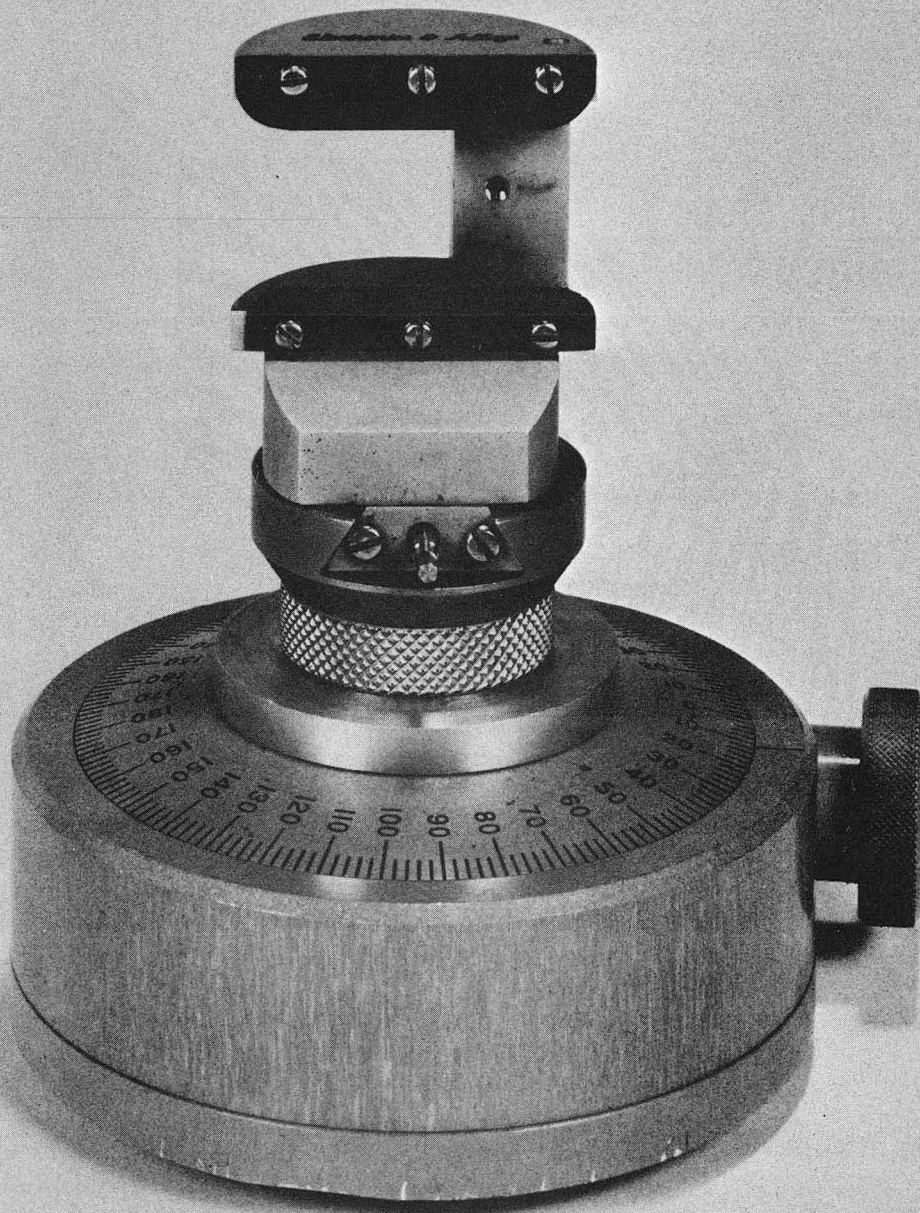
Fig. 6a
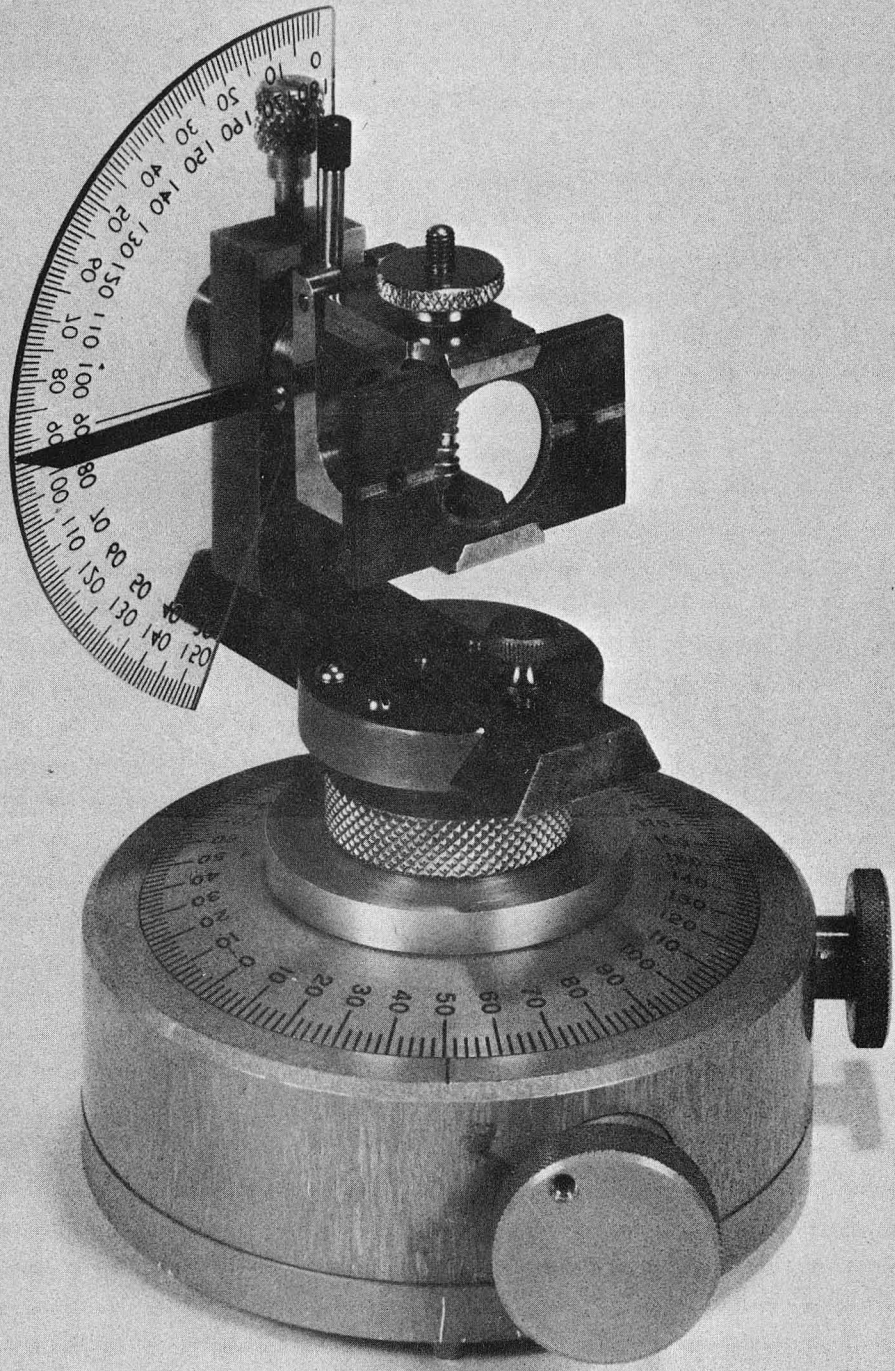
XBB 776-5964

Fig. 6b
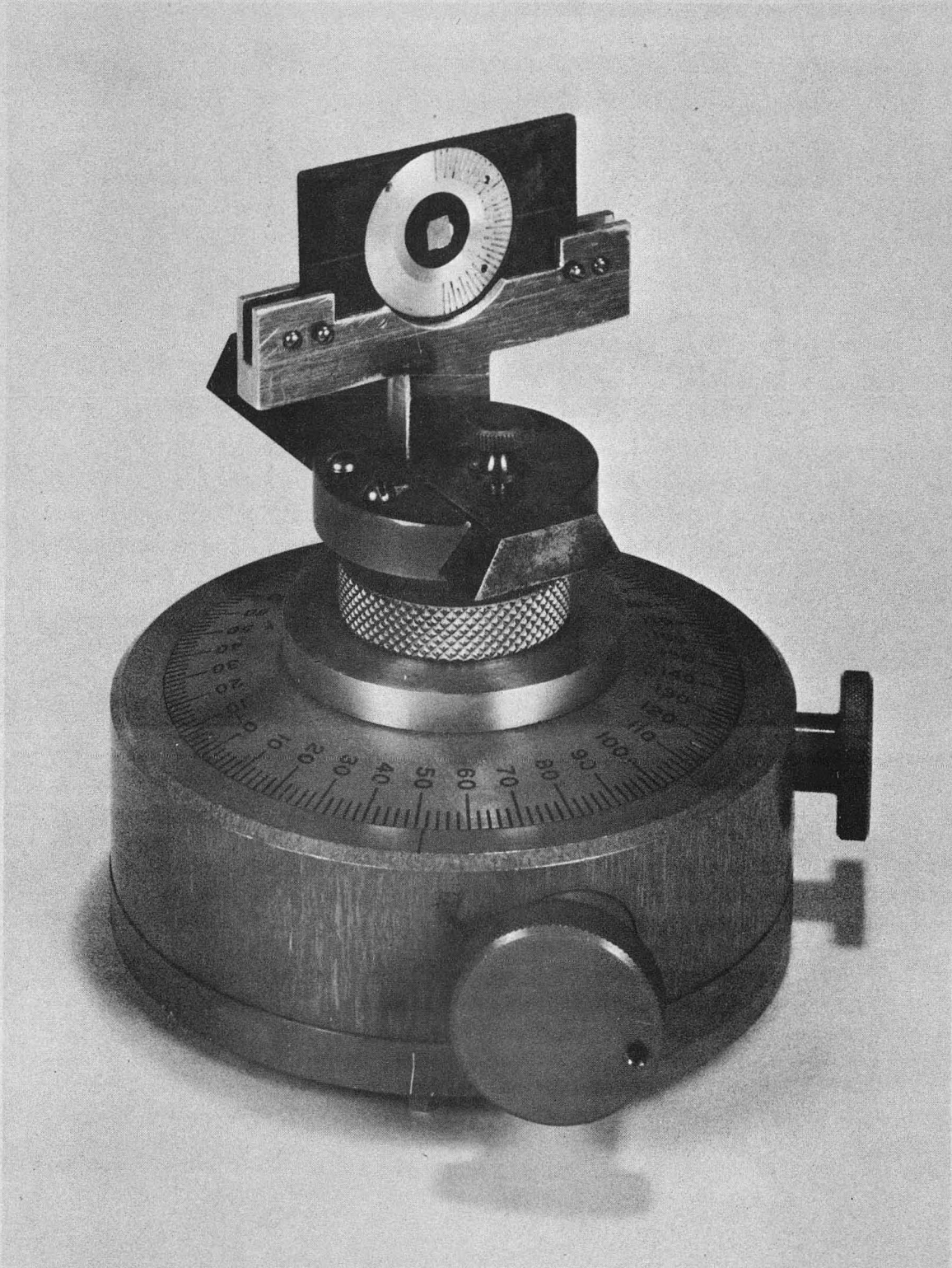
Fig. 6c

CBB 776-6025

Fig. 6d

58

(a)

(b)   (c)

SPECIMEN

(d)

1 cm
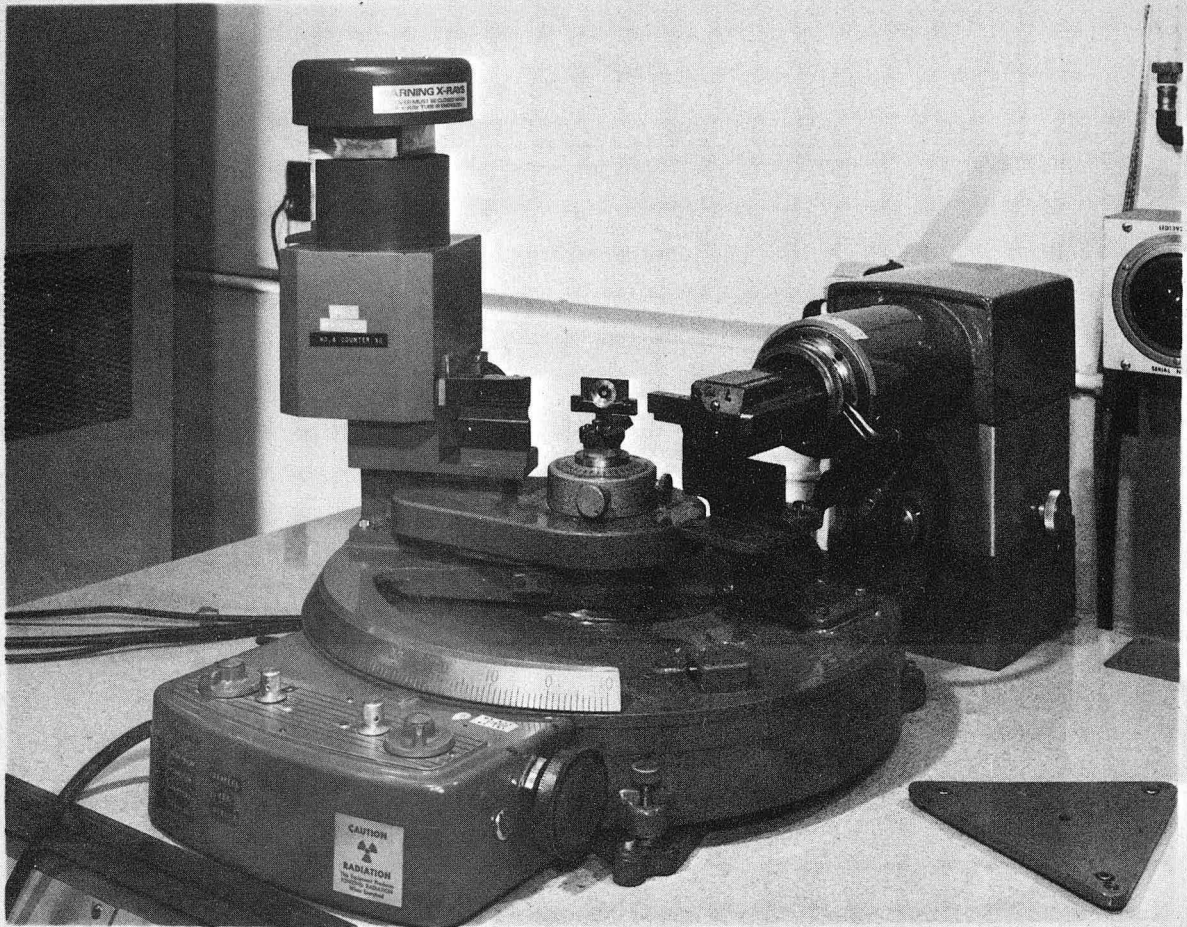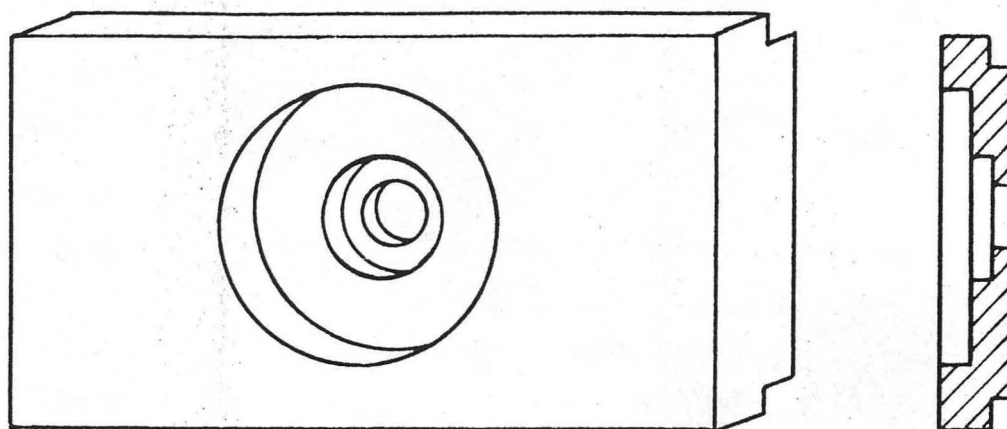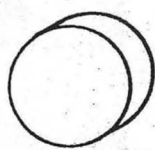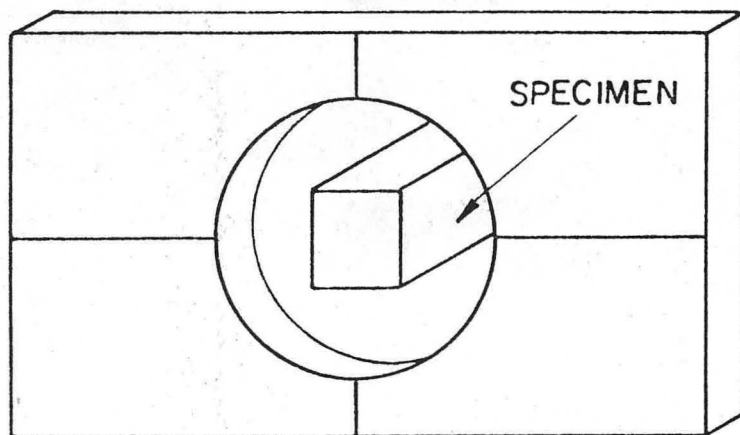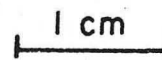
FIG. 7
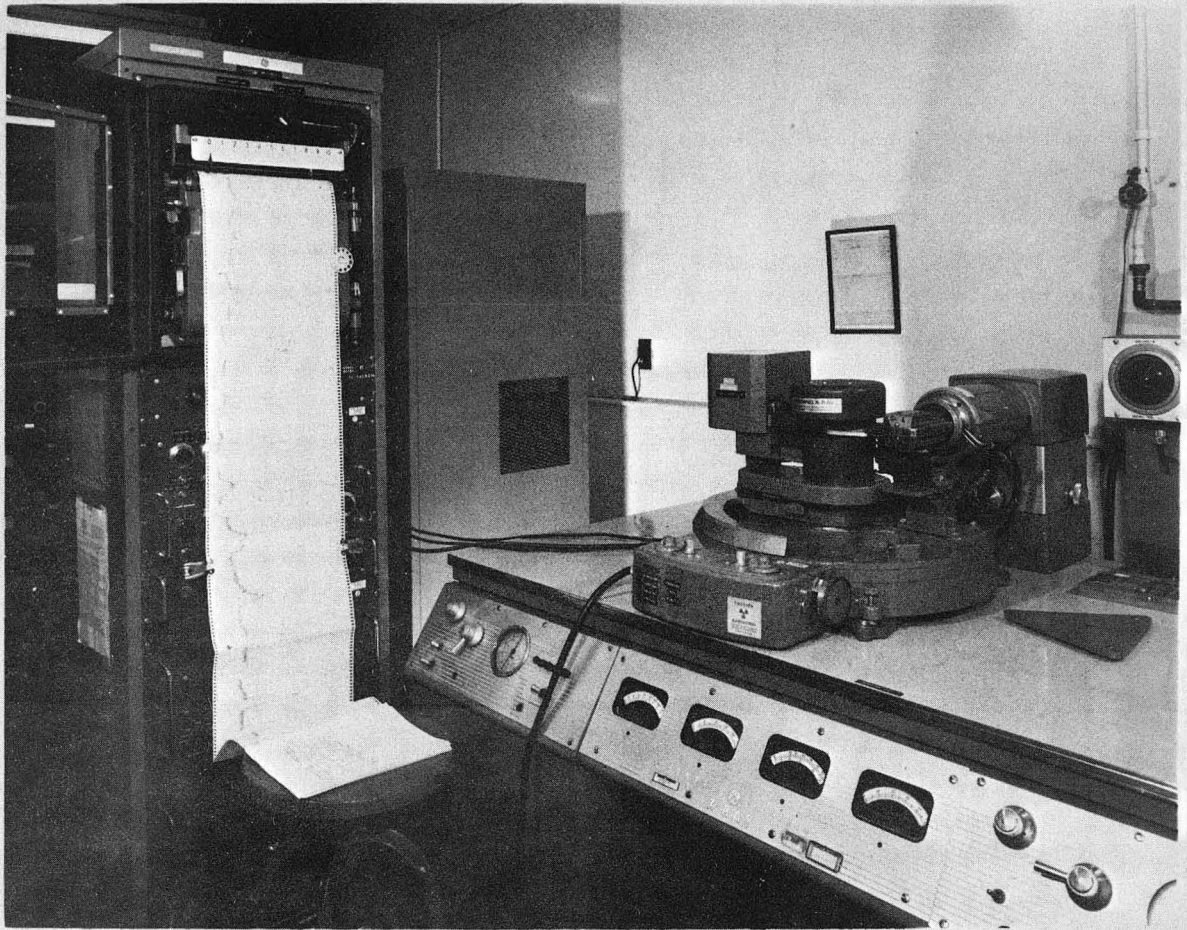
XBL 7712-6599

CBB 776-6023

Fig. 8
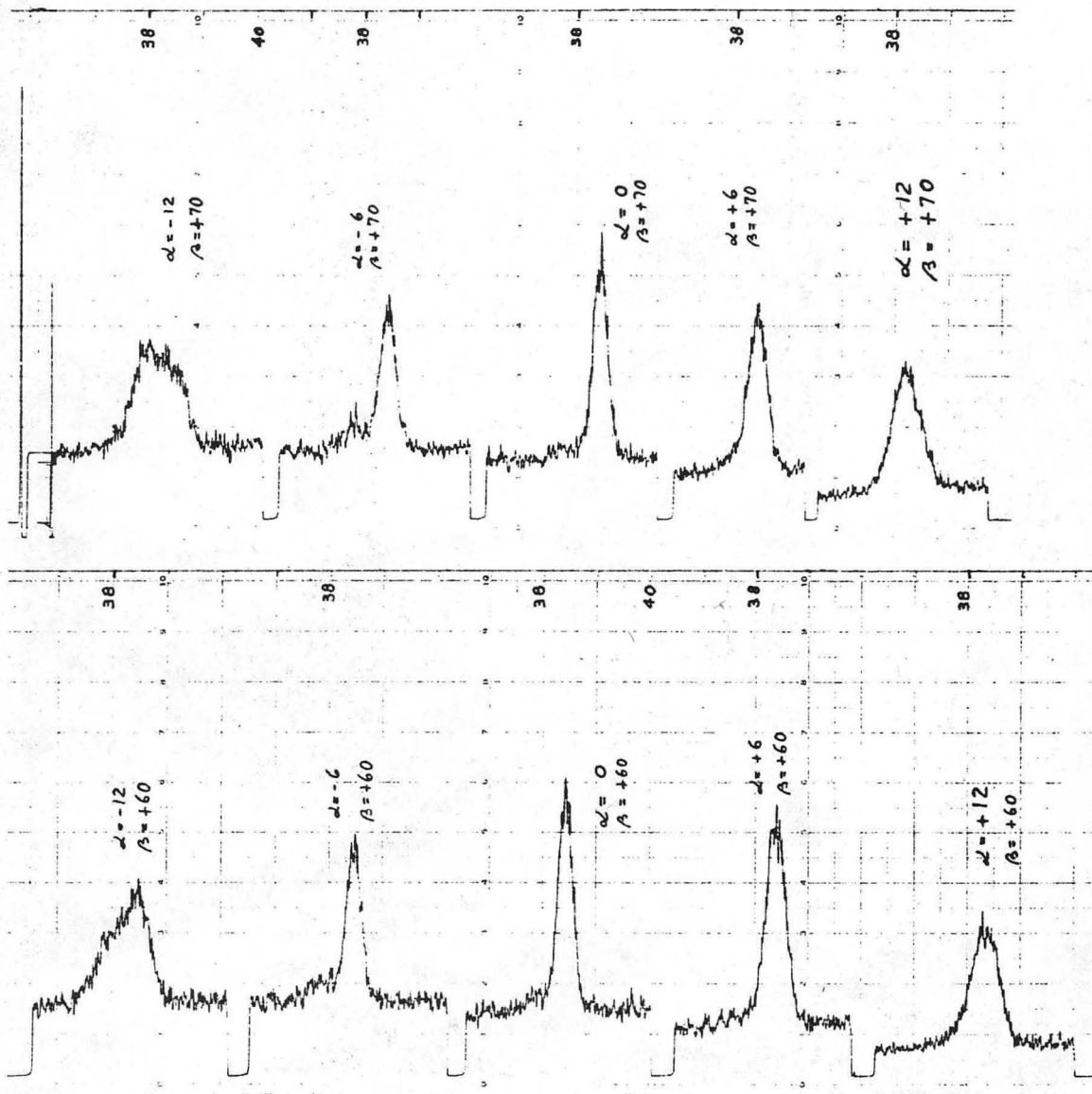
XBL 776-9244

FIG. 9

XBL 776-9244A

FIG. 10

(121)θ — (III)κ

1:1   3/4:1   1/2:1
          (a)

1/3:1   1/4:1   1/6:1
            (b)

XBL 7712-6593

FIG. 11

63

β=40°   β=90°

β=30°   β=80°

β=20°   β=70°

X-RAY
BEAM

SPECIMEN

β=10°   β=60°

β=0°   β=50°

XBL 7712-6595

FIG. 12
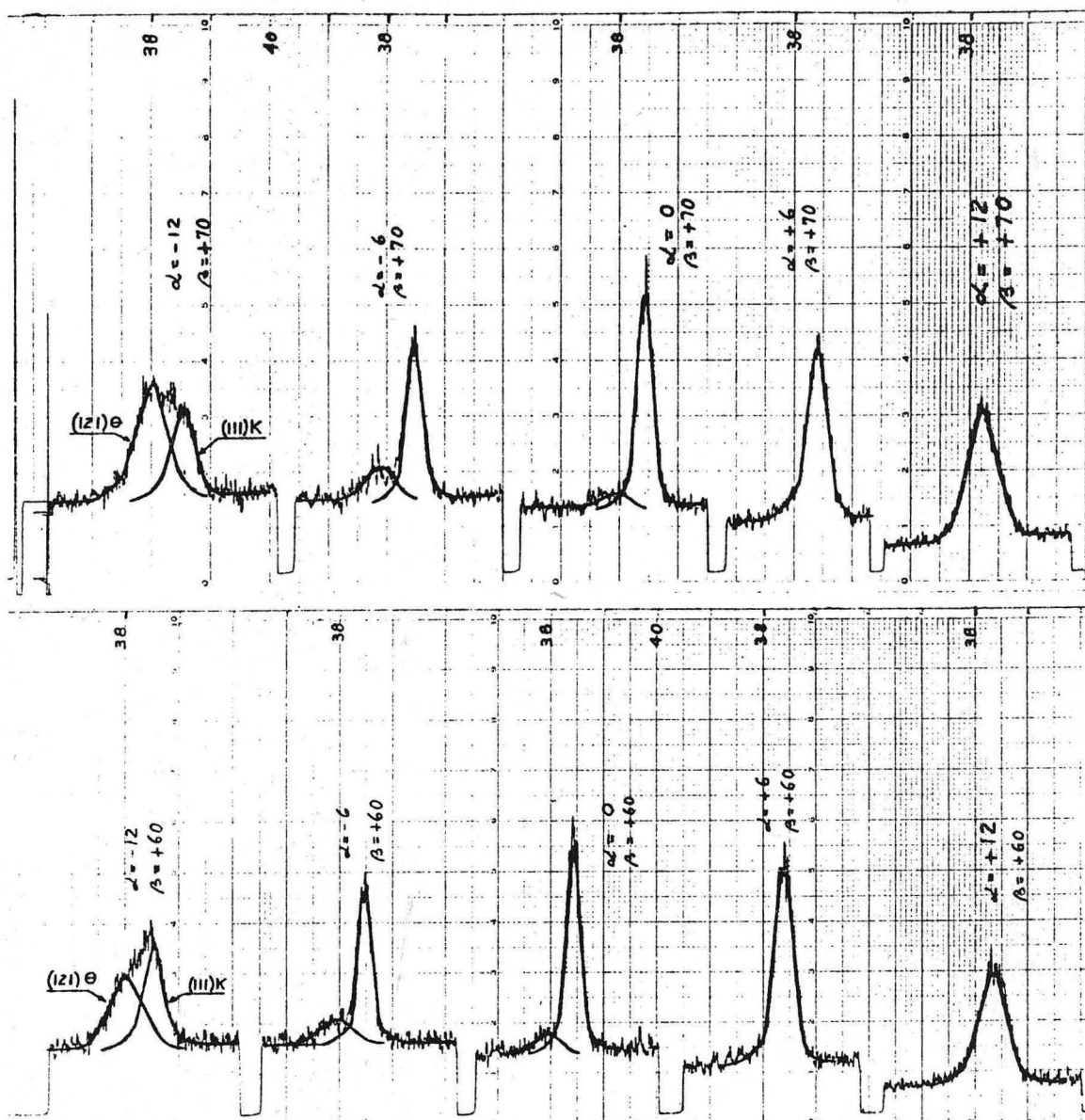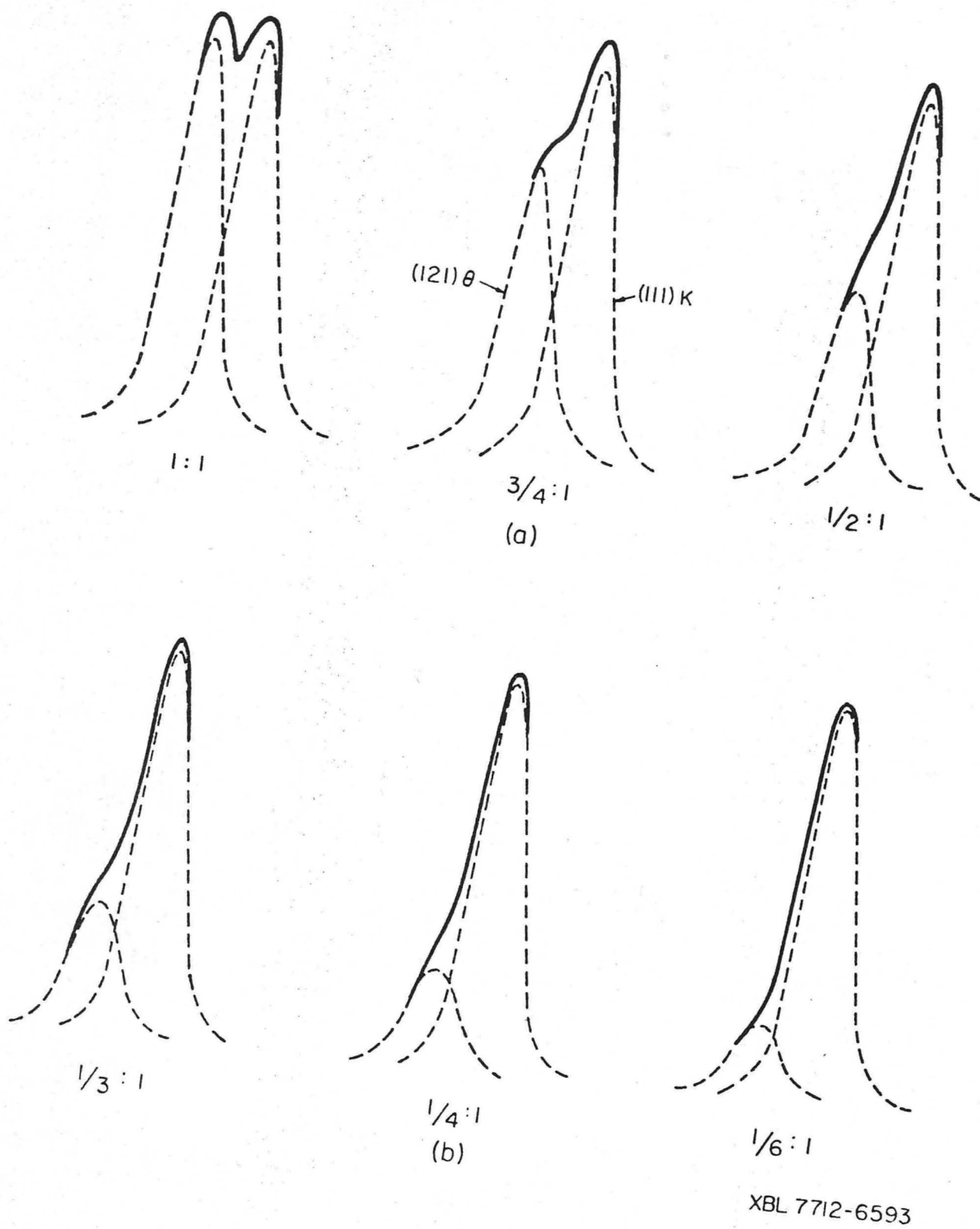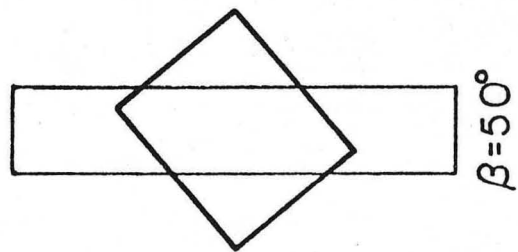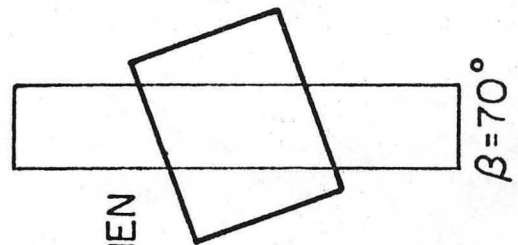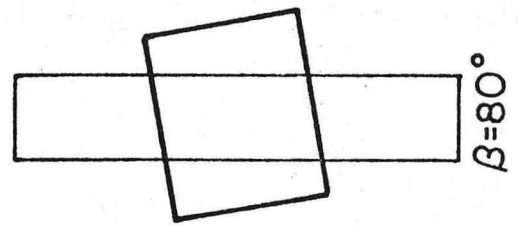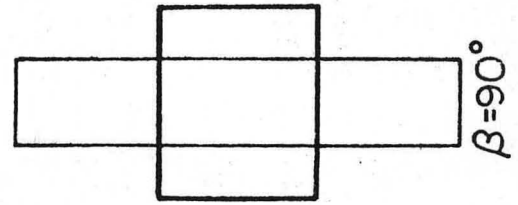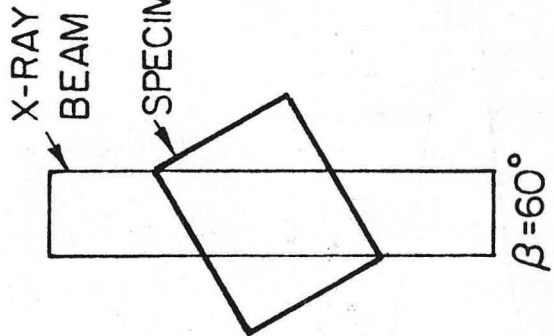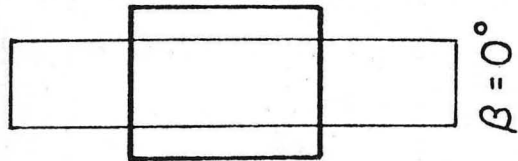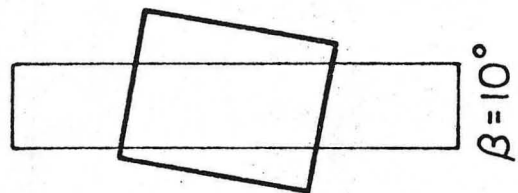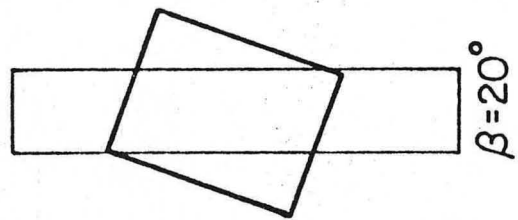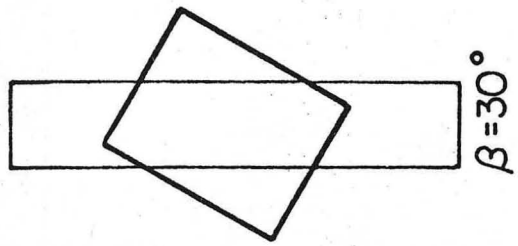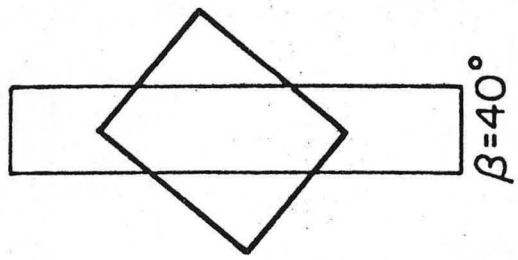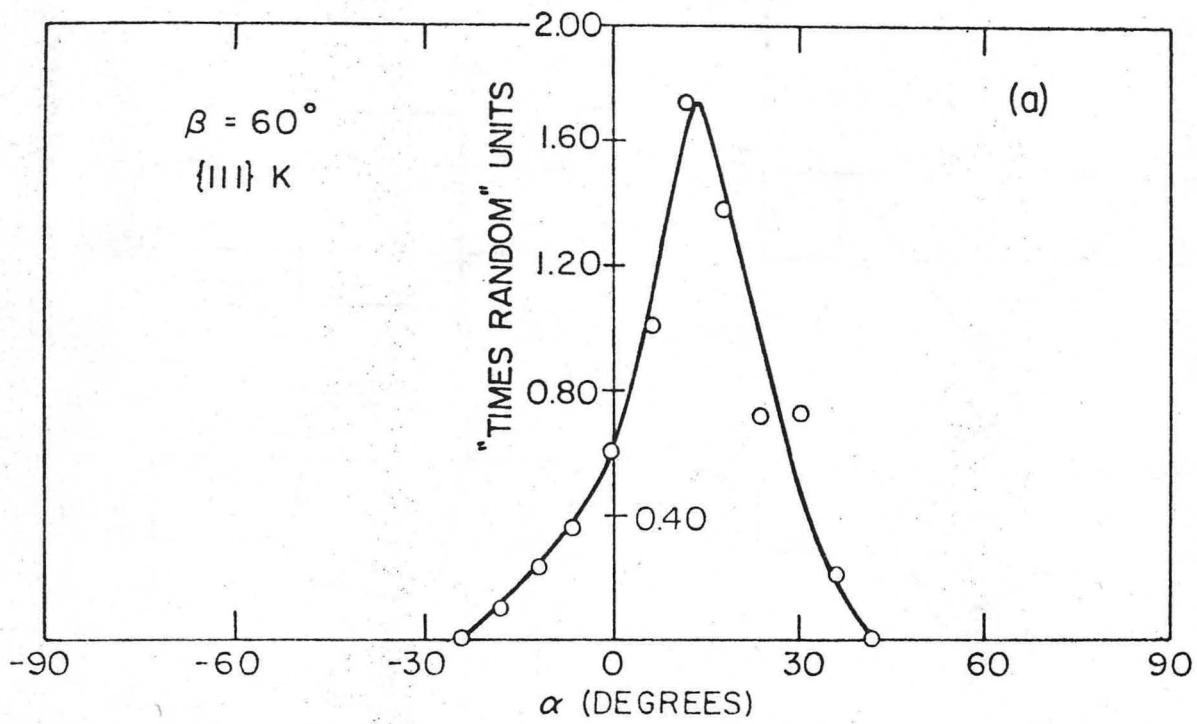
(a)
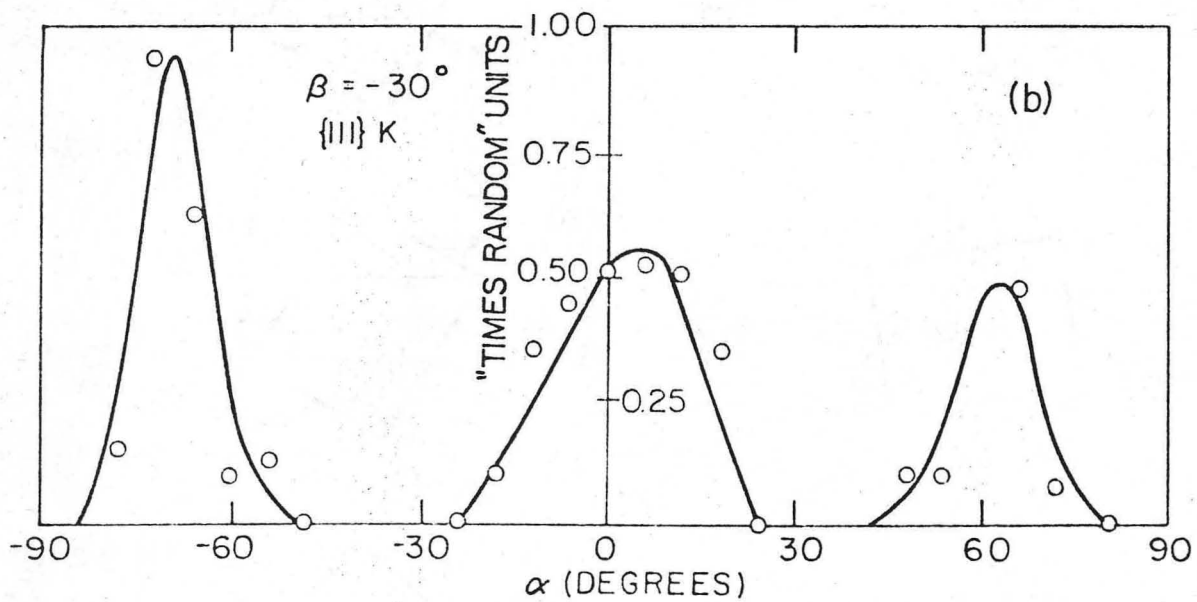
(b)

XBL 7712-6594

FIG. 13
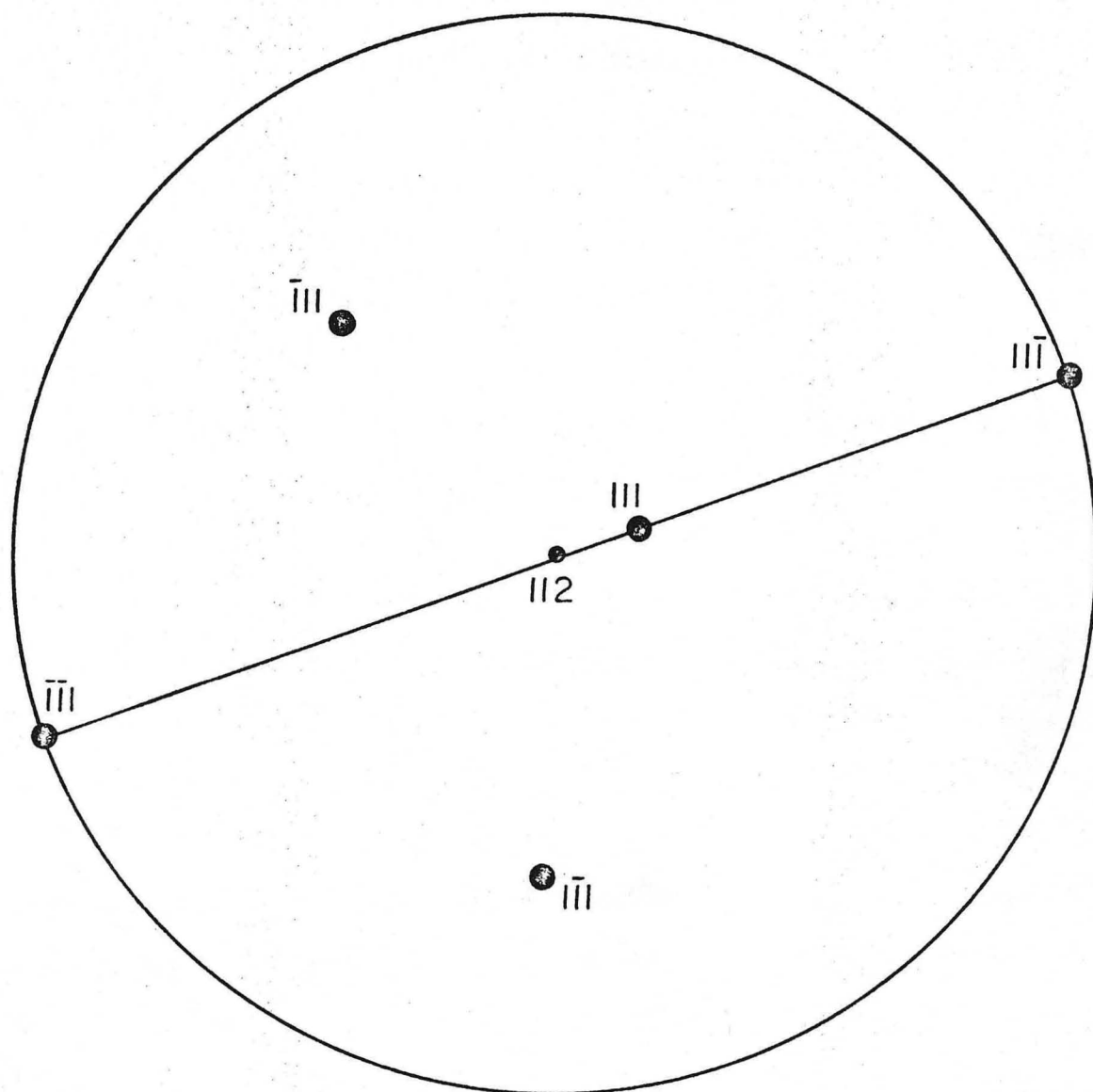
FIG. 14

XBL 7712-6598

INTENSITY LEVEL
"TIMES RANDOM" UNITS

O	0.50
△	1.00
□	2.50
▽	9.00
◇	12.00
●	MAX.

XBL 7712-6600

FIG. 15
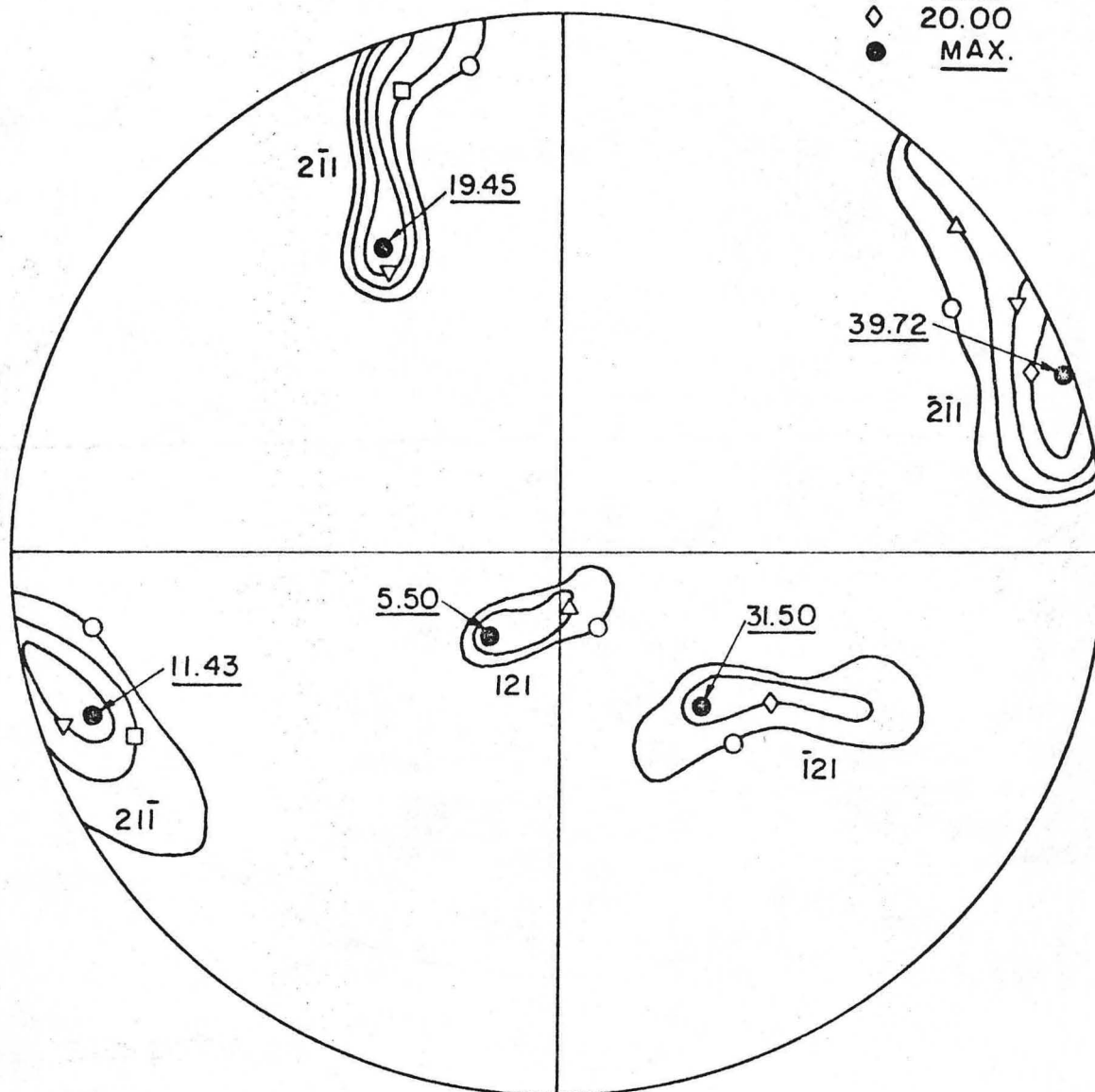
FIG. 16
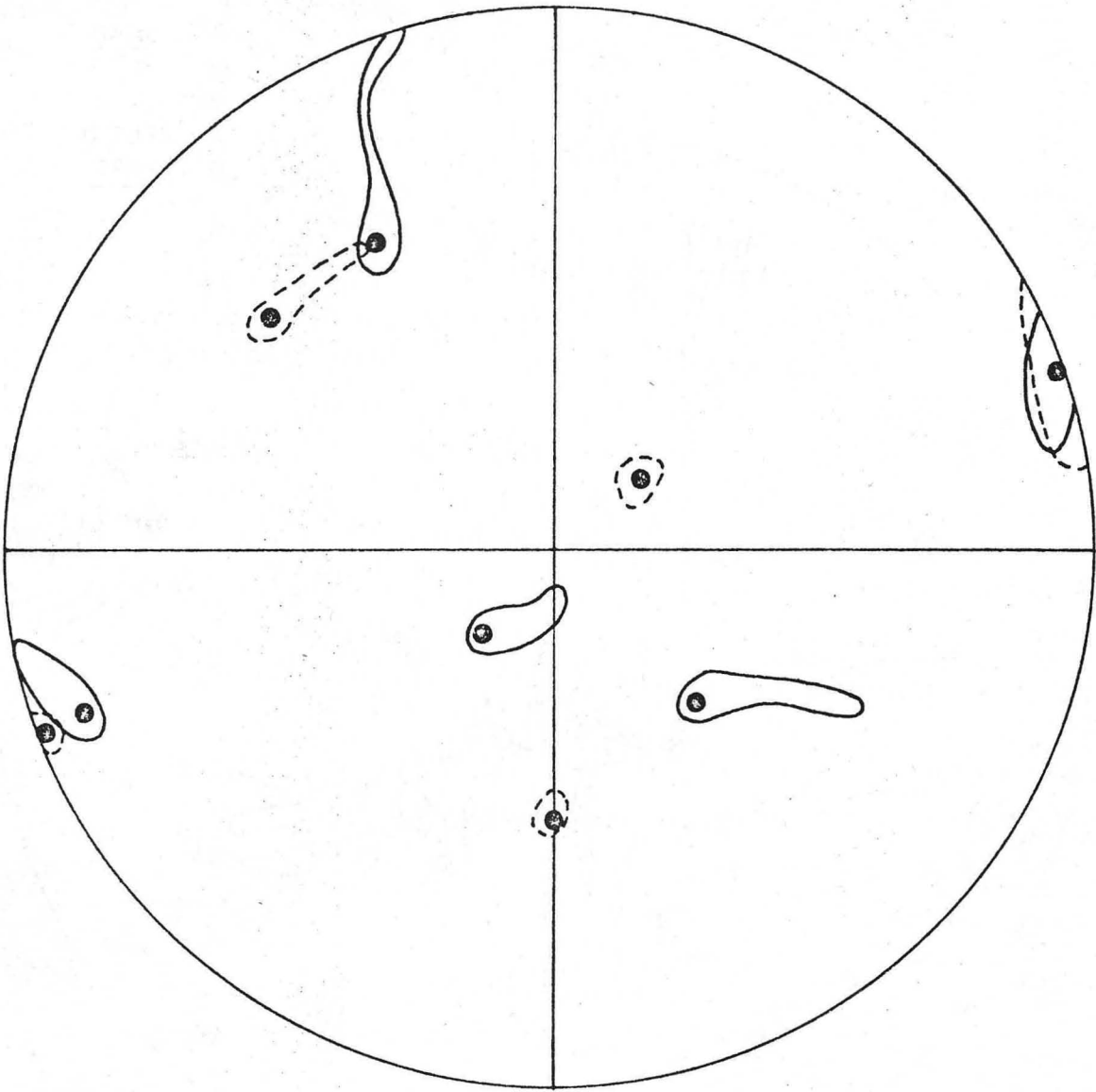
XBL 7712-6601

FIG. 17

XBL 7712-6602
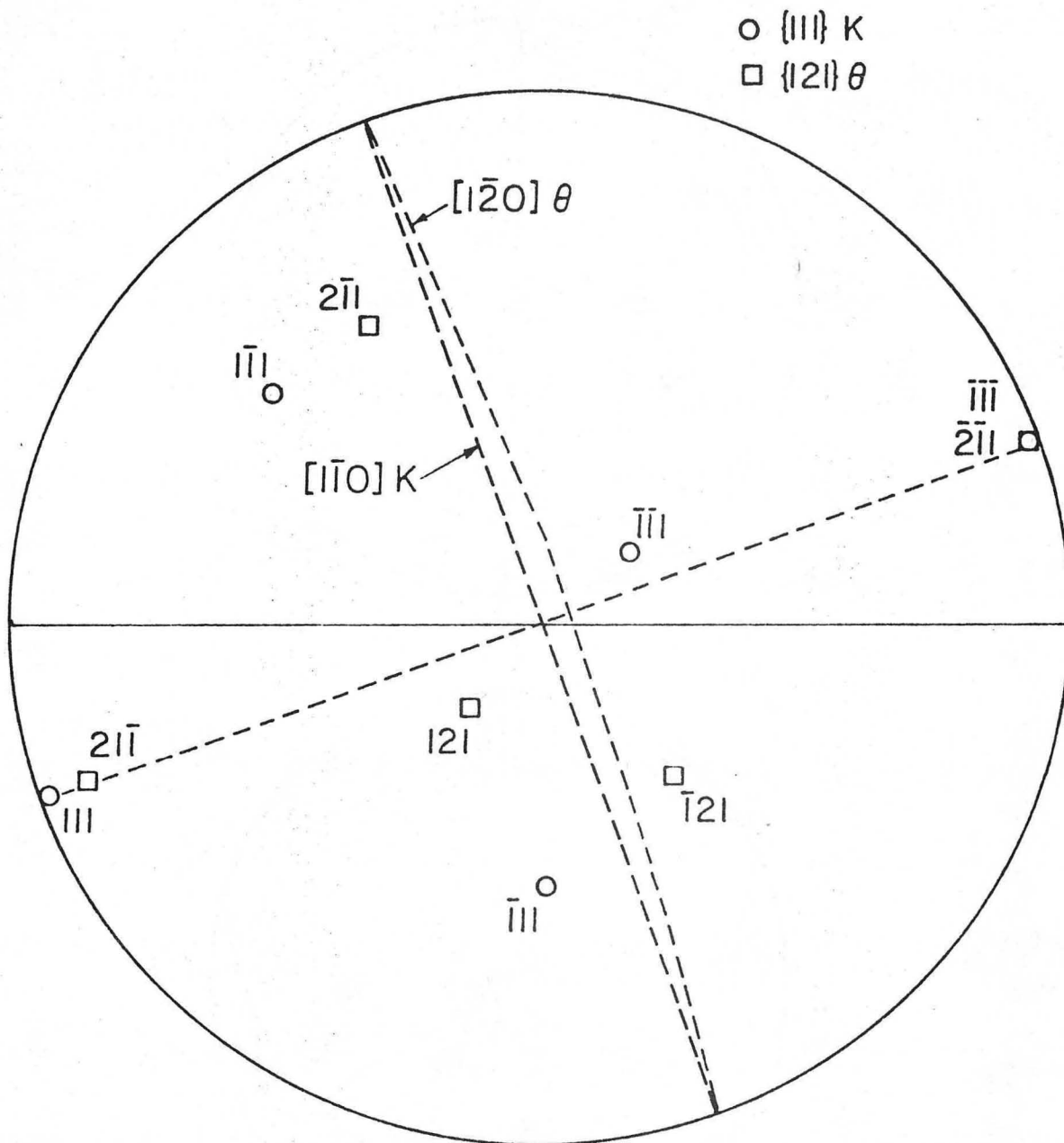
FIG. 18   XBL 7712-6596

(a)

(b)
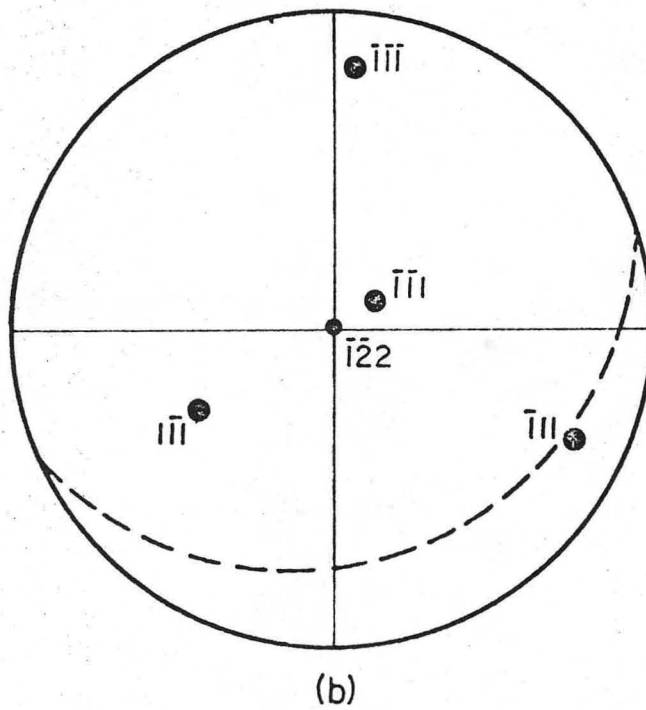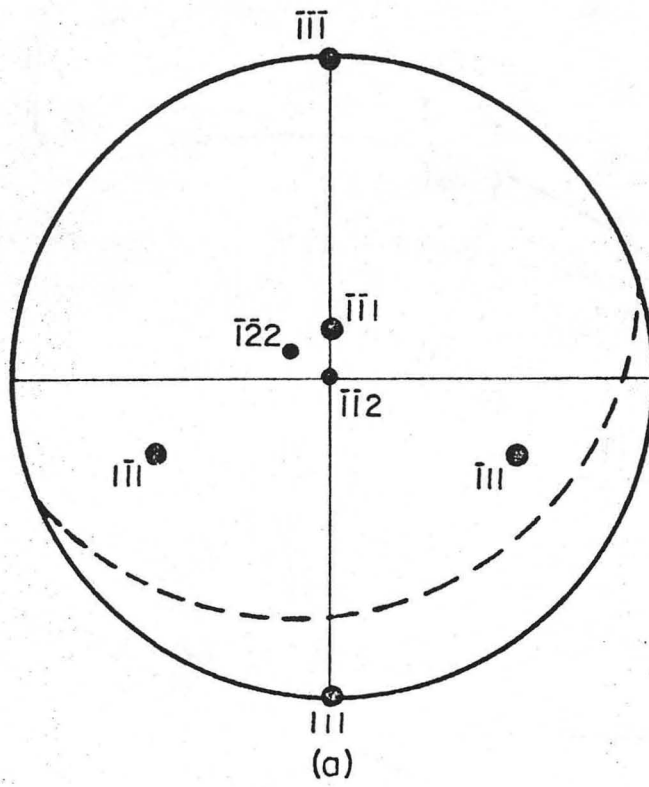
XBL 7712-6597

FIG. 19
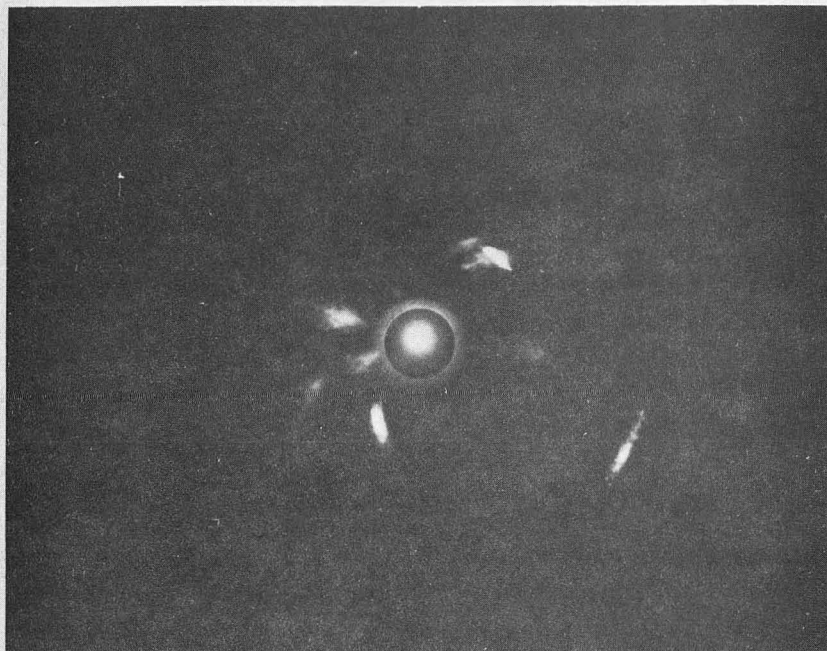
(a)
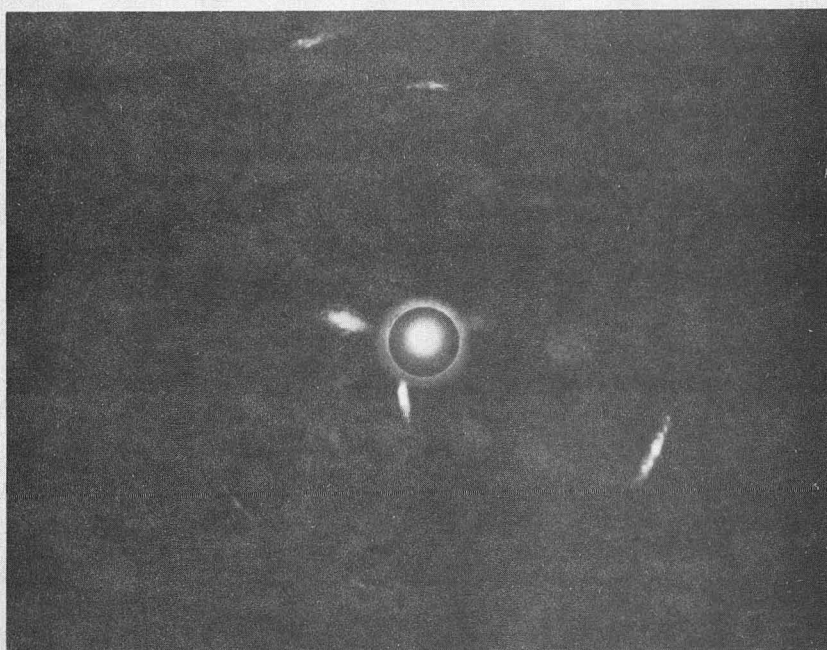
(b)   XBB 770-13049

Fig. 20

(a)

(b)

XBB 770-13048

Fig. 21